UCRL-8778

Physics and
Mathematics

UNIVERSITY OF CALIFORNIA

Lawrence Radiation Laboratory
Berkeley, California

Contract No. W-7405-eng-48

POSITIVE-PION PRODUCTION BY NEGATIVE PIONS

Walton A. Perkins III
(Thesis)

June 4, 1959

Printed for the U. S. Atomic Energy Commission

DISCLAIMER

POSITIVE-PION PRODUCTION BY NEGATIVE PIONS

Contents

ABSTRACT

A liquid hydrogen target was bombarded by negative pions of energies 260, 317, 371, and 427 Mev. Positive π mesons from the reaction $\pi^- + p \rightarrow \pi^+ + \pi^- + n$ were detected by using a counter telescope which selected the π^+ by its characteristic π-μ decay. With the 260-Mev beam π^+ mesons were counted at 90° in the laboratory system. At 317, 371, and 427 Mev the differential cross section was measured for π^+ mesons emitted at 60°, 90°, 125°, and 160° in the barycentric system. The angular distributions are nearly isotropic at 317 and 371 Mev but are peaked forward at 427 Mev. The total cross sections are: 0.14 ± 0.10 mb at 260 Mev; 0.71 ± 0.17 mb at 317 Mev; 1.93 ± 0.37 mb at 371 Mev; and 3.36 ± 0.74 mb at 427 Mev. These results indicate a much larger cross section than the theoretical prediction based on the static model. Reasonable agreement can be obtained by the inclusion of a pion-pion interaction in the production mechanism. (auth)

I. INTRODUCTION

In the study of the properties of the π meson, one of the important reactions is the production of pions by pions from hydrogen. The single-meson-production reactions

$$\pi^+ + p \rightarrow \pi^+ + \pi^+ + n,$$

$$\pi^+ + p \rightarrow \pi^o + \pi^+ + p,$$

$$\pi^- + p \rightarrow \pi^o + \pi^- + p,$$

$$\pi^- + p \rightarrow \pi^+ + \pi^- + n,$$

have been studied in emulsions,[1-5] in hydrogen diffusion cloud chambers,[6-8] in bubble chambers,[9-11] and recently with counters.[12] Most of this work was done in the 1-Bev region (i.e. with incident pions of kinetic energy of 1 Bev in the laboratory system).

Theoretical calculations for the above processes by Barshay,[13] Franklin,[14] Rodberg,[15] and Kazes[16] are an extension of the Chew-Low formalism for meson scattering to the process of meson scattering with production. This theory calculates the p-wave production in the one-meson approximation with an extended stationary nucleon and is not expected to be applicable at high energy. Indeed if the results of the theory are extrapolated to high energy[15] they predict cross sections which are much too small.

There is some evidence[12] of a disagreement with theory in the energy region near threshold, but the results are not conclusive. With this in mind we undertook the study of the process $\pi^- + p \rightarrow \pi^+ + \pi^- + n$ in the energy region from 260 to 430 Mev. The π^+ meson in the final state provides a unique signature for this reaction. The reactions in which two secondary pions are produced can be neglected because the highest energies are just barely above the energetic threshold of 360 Mev, and even at higher energies these cross sections are very small.[10] The positive pion which must be produced in a production process was unambiguously identified by its characteristic π-μ decay.

A large difference between experiment and theory might show a need for the inclusion in the theory of nucleon recoil or a pion-pion interaction. However, in this energy region one does not expect nucleon recoil to be important enough to account for any large discrepancy.

II. EXPERIMENTAL ARRANGEMENT

A. Magnets

A diagram of the experimental arrangement is shown in Fig. 1. The 730-Mev proton beam of the Berkeley synchro-cyclotron struck an internal beryllium target which was 2 in. thick in the beam direction. Negative pions were deflected by the cyclotron magnetic field and passed out of the vacuum tank through a thin aluminum window. The pions were next focused by a two-section quadrupole magnet with an aperture of 8 in.

After traversing an 8-ft. iron collimator, the pion beam was bent through 55° by a wedge magnet. The entrance and exit angles were chosen[17] to give equal horizontal and vertical focusing (assuming a parallel incident beam). The three-section 8-in. quadrupole magnet was used for fine adjustments in focusing the beam.

Wire-orbit measurements were made to determine the current settings for the pion beams of various energies. In principle the currents necessary for the quadrupoles could also be determined by the wire-orbit measurements. However, since it was impossible to extend the wire inside the cyclotron vacuum tank, this method did not work. Thus the quadrupole currents were varied experimentally to maximize the beam intensity. The first two-section quadrupole increased the beam intensity by a factor of 2.5 while the three-section quadrupole increased the intensity by approximately 50%. A pion beam intensity equal to or greater than 10^4/sec through a 2-in.-diameter counter (Counter 2 in Fig. 1) was available at all the energies used. A photograph of part of the experimental arrangement is shown in Fig. 2.

B. Pion Beams

Four negative pion beams were used with kinetic energies, energy spreads, and contaminations as listed in Table I.

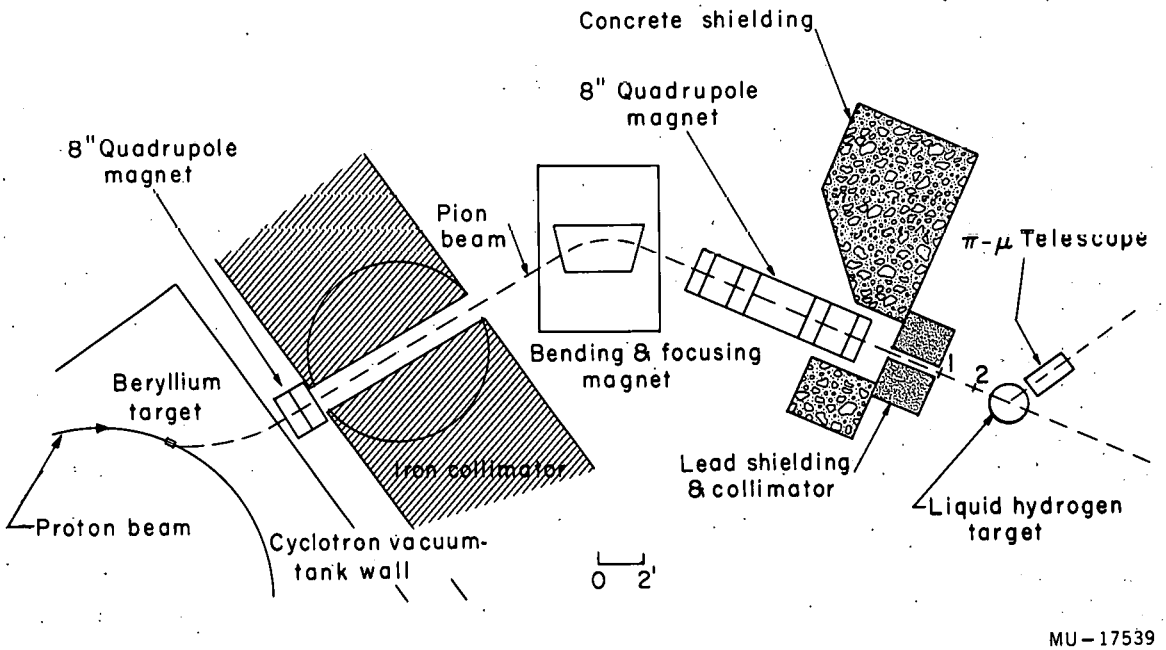

Fig. 1. Diagram of experimental arrangement.

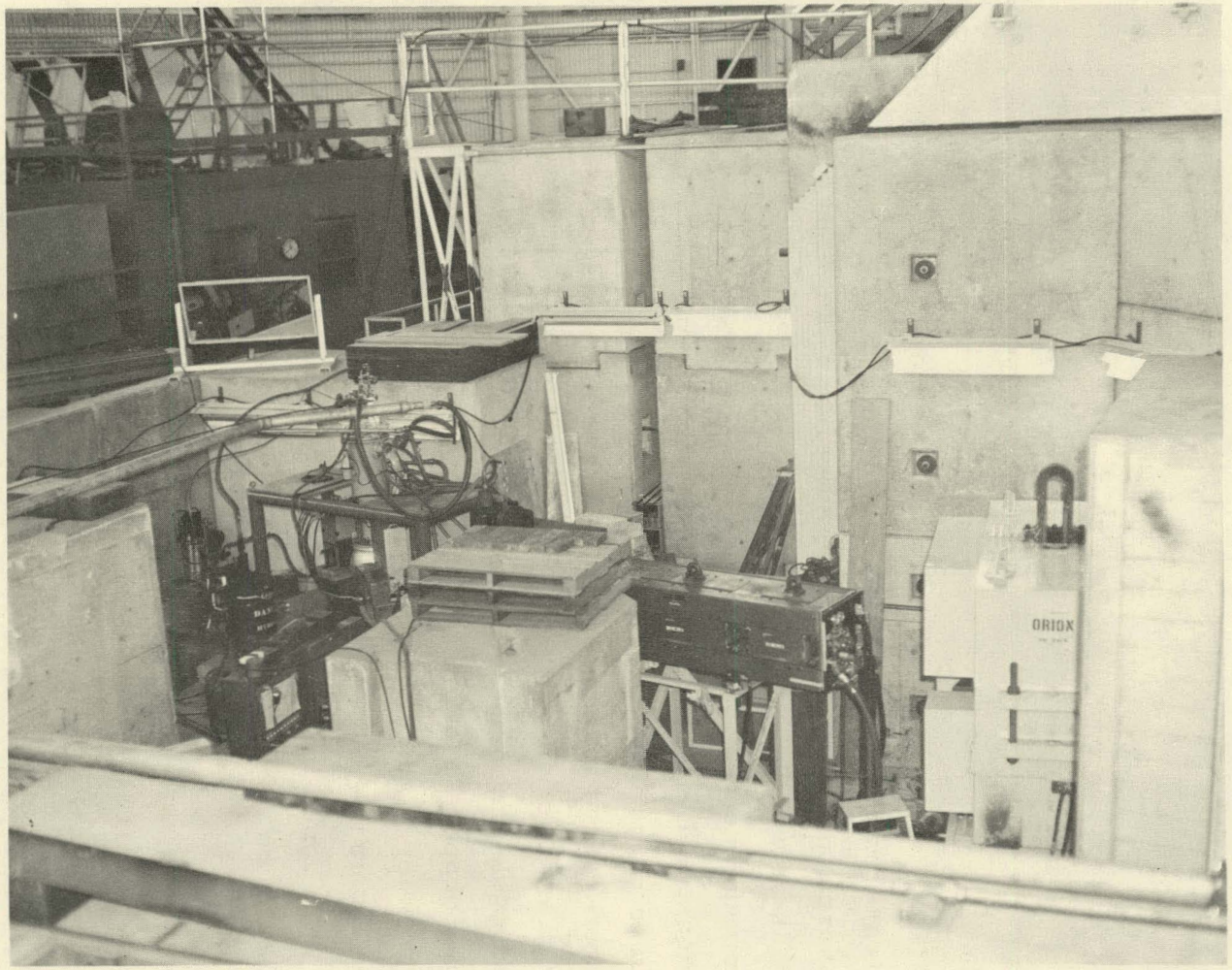

ZN-2155

Fig. 2. Part of the experimental arrangement.

Table I

Characteristics of π^- beams used

T_1 (Mev)	ΔT_1 (Mev)	%Muons	% electrons (upper limit)
260	7	11 ± 2	5
317	9	7 ± 2	3
371	11	4 ± 2	2
427	11	4 ± 2	2

The energies and energy spreads were determined from the range curves. Figures 3 and 4 are the 371-Mev range curves. Note the integral range curve, Fig. 3; A is the break between the pion-absorption loss curve and the stopping of the pions, and B is the break between the pions and the muons. Point B is used to determine the muon contamination from pions that decay before the bending magnet and that fraction of the muons formed after the bending magnet whose range is greater than 230 g/cm^2 Cu. The contamination of lower-energy muons produced after the bending magnet was determined by calculation to be about 1% for all energies used. Another correction was made for muon losses due to multiple Coulomb scattering in the thick copper absorber. (For the method used to calculate multiple scattering in thick absorbers in which energy loss is not negligible, see Appendix, page 52.)

An upper limit for the electron contamination was obtained by calculation. It was shown that charge exchange in the lead collimator, followed by $\pi^o \rightarrow 2\gamma$ and $\gamma \rightarrow e^+ + e^-$, would lead to less than 0.5% electron contamination. Another source of electrons was π^o production by protons in the internal beryllium target of the cyclotron. By making all assumptions in the direction to overestimate the electron contamination, the upper limits given in Table I were obtained. No electron-contamination correction was applied to the data, and the upper limits gave an uncertainty that was negligible in comparison with the statistical accuracy. (For more information on the method used to analyze range curves, see Appendix, page 47.)

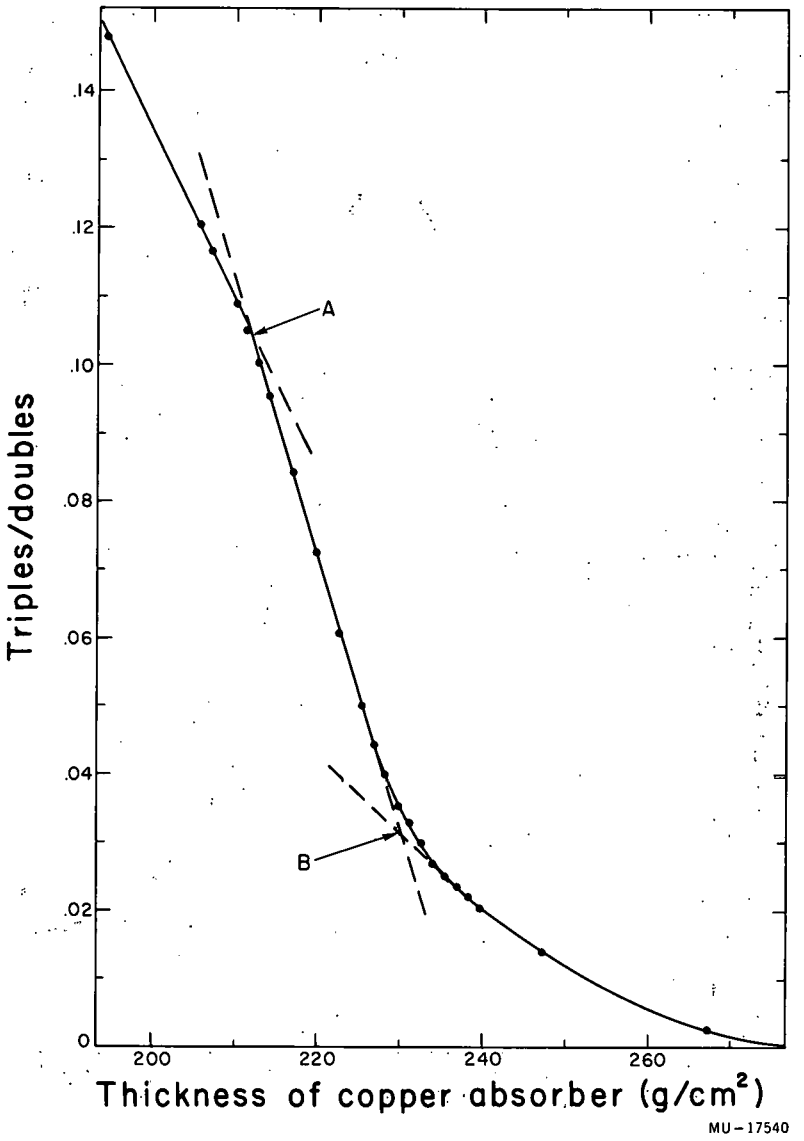

Fig. 3. Integral range curve for 371-Mev negative pion beam.
(See text for explanation of Points A and B.)

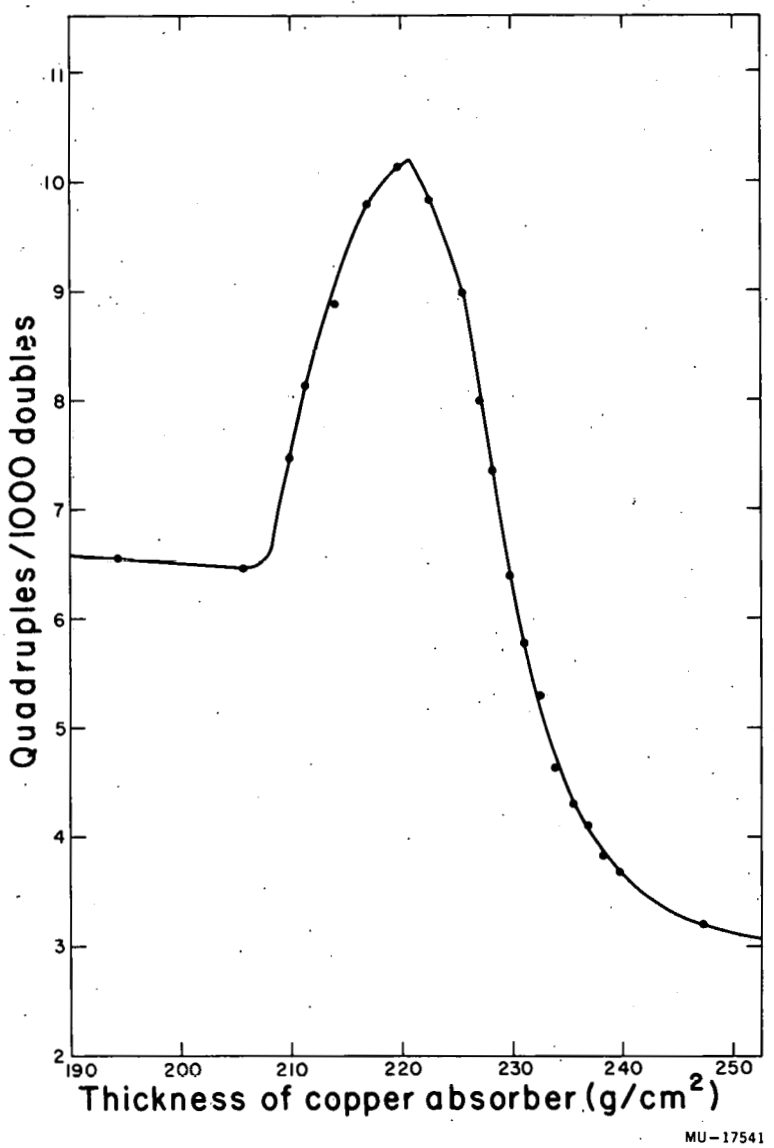

Fig. 4. Differential range curve for 371-Mev negative pion beam.

Horizontal and vertical profiles of the beam were taken with a 1-in.-diameter counter at the position of the liquid hydrogen target. These profiles are shown in Fig. 5. The beam was monitored with Counters 1 and 2. Triples refers to a triple coincidence between 1, 2, and the 1-in.-diameter counter.

C. Counters

A detail drawing of the hydrogen target and counter arrangement is shown in Fig. 6. All counters were made by using a plastic scintillator material consisting of a solid solution of terphenyl in polystyrene. Counter 1 was 3 by 3 in. and 0.25 in. thick, and Counter 2 was a 2-in.-diameter disk, 0.25 in. thick. Counter 3 was 6 by 6 in. 0.5 in thick; Counter 4 was 6 by 6 in., 2 in. thick; and Counter 5, the anticoincidence counter, was 6 by 7 in., 0.5 in. thick, with 0.5-in. overlapping lips on three sides. Counters 3, 4, and 5 compose the π-μ counter telescope.

For the range-curve measurements, copper absorbers were placed after Counter 2, followed by Counters 6 and 7 in that order. Counter 6 was a 6-in.-diameter disk, 0.5 in. thick, and Counter 7 was a 12-in.-diameter disk, 1 in. thick.

Counters 1, 2, 4, 6, and 7 were viewed by 6810A photomultiplier tubes, while Counters 3 and 5 were viewed by 6199 photomultiplier tubes. The response over the surface of Counters 3 and 4 was tested with a radioactive beta source and was found to be uniform within $\pm$ 25 volts on the photomultipliers' high-voltage supplies. The center of Counter 4, which defined the solid angle, was 16.1 in. from the center of the liquid hydrogen target.

D. Electronics

A block diagram of the electronics is shown in Fig. 7. The high counting rate in the monitor--sometimes as great as 2×10^{4}/sec meant that the counters and electronics had to be built for high-speed counting rates. The synchrocyclotron repetition rate is 64 pulses per second, of width ~400μsec. These pulses have a fine structure of short pulses (1×10^{-8} sec), 5.4×10^{-8} sec apart, due to the

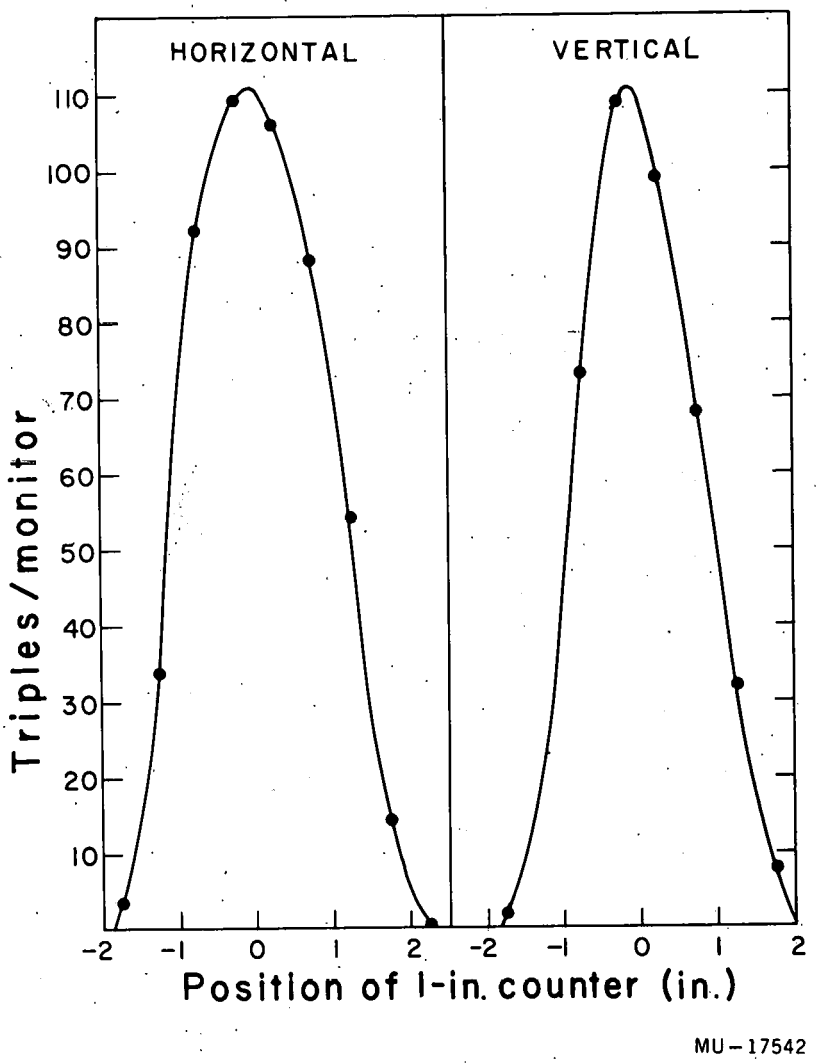

Fig. 5. Horizontal and vertical beam profiles taken with a 1-in.-diameter counter at the position of the liquid hydrogen target.

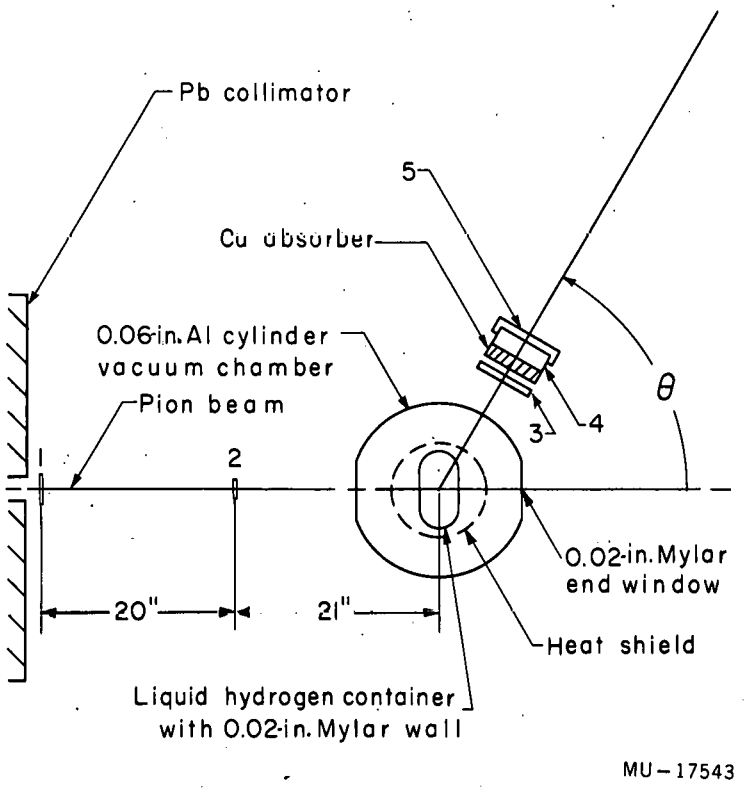

Fig. 6. Diagram showing details of hydrogen target and counter arrangement.

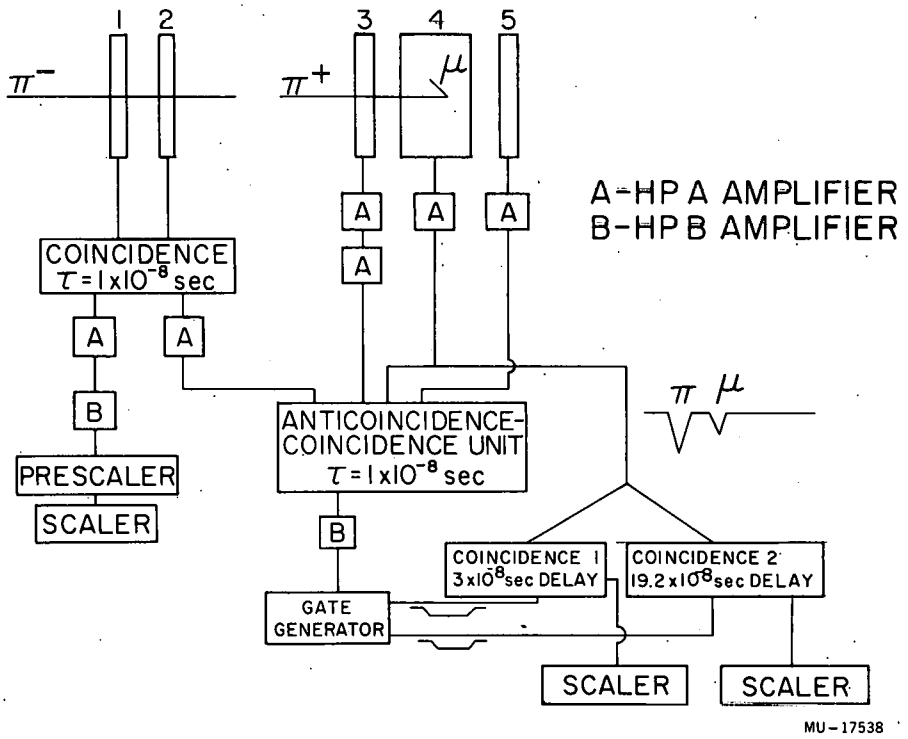

Fig. 7. Block diagram of electronics for monitor and π-μ telescope.

phase-stability bunching of the accelerated protons. Even with the best electronics now available it is impossible to resolve and count two particles in the same fine-structure pulse. During the large pulses, which occurred 64 times per second, the equipment had to be able to handle a counting rate of 10^6 pulses per second.

To maintain 4-volt output pulses the counters' photomultiplier tube bases needed large capacitors (1μf in the last stage) so that the voltage across the dynodes would not drop more than 1% during the 400-μsec pulses. The Evans coincidence circuits,[18] which have a resolving time of about 1×10^{-8} sec, were tested with a pulser and shown to be capable of uniform performance at 10 megacycles operating continuously. The Hewlett-Packard decade prescalers were also capable of continuous operation at 10 Mc. The Hewlett-Packard 460A distributed amplifiers were used for amplification, while the 460B distributed amplifiers were used for amplification and inversion of the pulses.

The identification of π^+ mesons was based on their mean life of 2.55×10^{-8} sec. This general method of positive-pion detection was originated by Chamberlain, Mozley, Steinberger, and Wiegand,[19] and has been used extensively in the past. A detailed description of this type of electronic equipment is given by Imhof, Kalibjian, and Perez-Mendez.[20]

The fourfold coincidence and anticoincidence $12345\bar{}$ initiated a gate of 6×10^{-8} sec duration, delayed approximately 3×10^{-8} sec relative to the initiating pulse. The coincidence between the gate and delayed pulse in Counter 4 was registered on a scaler. When this occurred, presumably a π^- meson traversed Counters 1 and 2, entered the H_2 target, producing the π^+ meson which passed through Counter 3, and stopped in Counter 4, generating the 6×10^{-8}-sec gate. Then the 4.1-Mev muon, from the π^+ decay, gave a delayed pulse which made a coincidence with the gate.

However, it was possible for two random particles or a μ-e decay to simulate this effect. The accidental and μ-e decay coincidences were monitored by using an identical coincidence channel in

which the gate delay was set at 19.2×10^{-8} sec. The muons were formed from pion decay in the counter and their subsequent electron decay led to a small error (2%) in monitoring the accidentals. Although slightly more μ-e decays occurred during the first gate, about 1/3 of these were concurrent with π-μ decays. This led to a slight overestimation of the accidentals.

The π^+ counting equipment did not respond to the other particles encountered during the experiment. For example, π^- mesons that stop in matter are almost always captured, and therefore have a mean life in scintillator material of approximately 10^{-11} sec.

The particles counted during the experiment were shown to have a mean life of $2.7 \pm 0.2 \times 10^{-8}$ sec by a least-squares fit to the data points plotted in Fig. 8. This is in satisfactory agreement with the accepted mean life for pions. For measuring the mean life, the electronics was slightly altered so that the output pulse of the 12345 coincidence triggered a cathode-ray oscilloscope (Tekronix 517). The pulses from Counter 4--see below--were displayed on the oscilloscope and photographed by a Dumont oscilloscope camera.

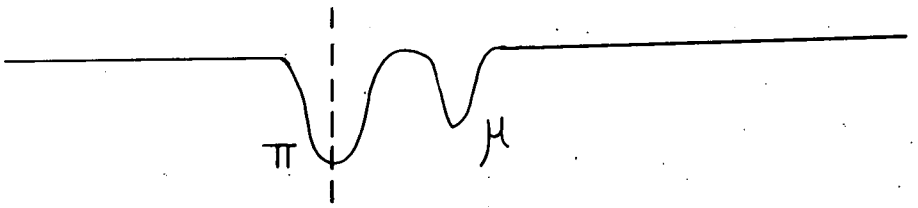

By photographing the events and measuring the separation between the pulses the integral decay curve shown in Fig. 8 was obtained.

Corrections have been applied for accidentals and π-μ-e decays for which the muon pulse could not be resolved from that of the pion. Accidentals were estimated by counting the number of events in which the μ pulse occurred before the π pulse, and this was found to be less than 10%. The π-μ-e decay correction was estimated by a simple calculation and was important only for large t.

Prior to the actual run, a calibration run (described in the Appendix) was taken in which the counter telescope was placed in a π^+-meson beam. A plateau in the counting rate as a function of high

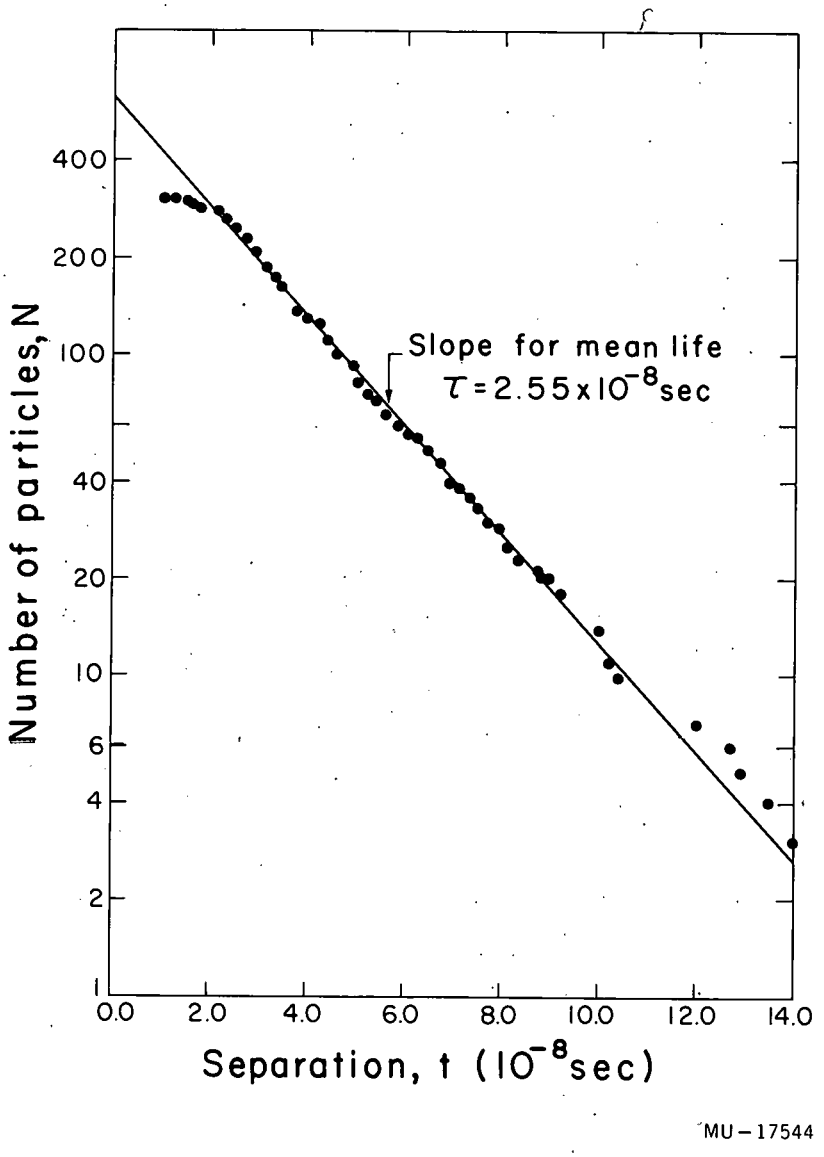

Fig. 8. Integral mean-life curve for particles produced by 371-Mev negative pions in liquid hydrogen target. Straight line is for $N = N_o e^{-t/\tau}$ with $\tau = 2.55 \times 10^{-8}$ sec.

voltage was observed for each counter. The counters were operated in the plateau region to insure stable operation of the electronics. Proper cable lengths between counters and electronic equipment were determined by observing the counting rate as a function of one counter's delay relative to all other counters. By varying the delay of the gate relative to the pulses in Counter 4, we measured the mean life of the particles that are counted in the counter telescope. (See Fig. 26 in Appendix.) The mean life agrees within statistics with the accepted value for π^+ mesons.

During the experiment it was necessary for "Coincidence 1" and "Coincidence 2" to be set at the same discrimination level in order that the accidental counts observed in Channel 2 be an accurate measure of those accepted by Channel 1. During the run this discrimination level was checked in two ways. First it was checked by feeding pulses to the "gate generator" from a 100-kilocycle pulser and adjusting the discriminators until equal numbers of "accidental" coincidences were observed in both channels. Secondly the counter telescope was placed in the direct π^- beam and the numbers of accidental coincidences in both channels were balanced. For correct operation both methods must give the same result; this they did. For the second method to show the correct discrimination-level balance, the difference in delay between the two gates must be an integral multiple of the separation between cyclotron fine-structure pulses ($19.2\times10^{-8} - 3\times10^{-8} = 3\times5.4\times10^{-8}$). Both checks were made daily during the course of the experiment.

$Ru^{106} - Rh^{106}$ beta sources were taped to Counters 3, 4, and 5. To insure stability of the equipment, singles counting rates of the beta sources were taken twice daily for each scintillator; only slight downward drifts in the gain of the Hewlett-Packard amplifiers were observed. These were compensated for by increasing the photomultiplier high voltages.

E. Target

The liquid hydrogen target used consisted of a large reservoir and a smaller target container. The small target container was suspended in the direct π^- beam. The large reservoir was surrounded by a liquid nitrogen container used as a heat shield and the whole assembly was in a vacuum. A cross-section view of the liquid hydrogen container and vacuum chamber is shown in Fig. 6.

The 4.5-in.-diameter Mylar end windows provided a thin, low-Z material in the direct beam and made possible visual observation of the liquid hydrogen container. The heat shield was a 0.001-in. aluminum foil in thermal contact with the liquid nitrogen reservoir. The liquid hydrogen container was made of 0.02-in.-thick 5-in.-wide Mylar sheet with copper top and bottom plates bonded with a Versamid-epoxy mixture. The shape of the Mylar sheet is shown in Fig. 6; the straight sections are 4 in., with arcs of 2-in. radii on the ends. The sides of the target, surrounded by vacuum, bow out slightly since the inside of the vessel is at atmospheric pressure. This bowing, a 7% effect, was measured experimentally and corrected for.

The liquid hydrogen container could be emptied or filled by closing or opening its venting line. The excess or deficit in liquid hydrogen was taken up or supplied by the reservoir.

F. Experimental Method

Since we are dealing with a three-body final state in the reaction under study ($\pi^- + p \rightarrow \pi^+ + \pi^- + n$), the π^+ in the center-of-mass system can have any energy from zero to some maximum energy. This maximum energy depends only on T_1, the kinetic energy of the incident π^- meson in the laboratory system. For a π^+ emitted at some angle θ^* in the barycentric system, its laboratory angle θ will depend on its barycentric kinetic energy T^*. Therefore, to count π^+ mesons at one angle and several energies in the barycentric system, it is necessary to use several angles in the laboratory system. Except for small T^* these angles are only a few degrees apart for the same θ^*. Before the experiment the lab angles and

energies were calculated from the chosen c.m. angles and energies. After the experiment, when all lab quantities were definitely known, a conversion from the laboratory to center-of-mass system was made, the results of which are given in Section IV, Table II. The relativistic equations that were coded for the I. B. M. 650 computer in order to solve this problem are as follows (all energies are in units of Mev;

E^*_T is the total center-of-mass energy,

M_π is the pion rest energy,

M_p is the proton rest energy,

M_n is the neutron rest energy,

T, P, E, T^*_{max}, P^*_{max} all refer to the π^+ meson.)

$$E^*_T = \left[(M_\pi + M_p)^2 + 2T_1 M_p \right]^{1/2} \tag{1}$$

$$\bar{\gamma} = (T_1 + M_\pi + M_p) / E^*_T \tag{2}$$

$$\bar{\eta} = \bar{\beta}\bar{\gamma} = \left[T_1 (T_1 + 2M_\pi) \right]^{1/2} / E^*_T \tag{3}$$

From center-of-mass system to laboratory system:

$$P^*_{max} = \frac{1}{2E^*_T} \left\{ \left[E^{*2}_T - (2M_\pi + M_n)^2 \right] (E^{*2}_T - M_n^2) \right\}^{1/2} \tag{4}$$

$$T^*_{max} = (P^{*2}_{max} + M_\pi^2)^{1/2} - M_\pi \tag{5}$$

$$T^* = fT^*_{max} \text{ for "f" from 0 to 1.0 in 0.1 increments} \tag{6}$$

$$E^* = T^* + M_\pi, \quad P^* = (E^{*2} - M_\pi^2)^{1/2} \tag{7}$$

$$P^2 = (\bar{\gamma} P^* \cos\theta^* + \bar{\eta} E^*)^2 + (P^* \sin\theta^*)^2 \tag{8}$$

$$T = (P^2 + M_\pi^2)^{1/2} - M_\pi \tag{9}$$

$$\theta = \tan^{-1}\left[P^*\sin\theta^*/\left(\overline{\gamma}P^*\cos\theta^* + \overline{\eta}\,E^*\right)\right] \tag{10}$$

From laboratory system to center-of-mass system:

$$E = T + M_\pi, \quad P = (E^2 - M_\pi^2)^{1/2} \tag{11}$$

$$P^{*2} = (\overline{\gamma}P\cos\theta - \overline{\eta}\,E)^2 + (P\sin\theta)^2 \tag{12}$$

$$T^* = (P^{*2} + M_\pi^2)^{1/2} - M_\pi \tag{13}$$

$$\theta^* = \tan^{-1}\left[P\sin\theta/\left(\overline{\gamma}\,P\cos\theta - \overline{\eta}\,E\right)\right] \tag{14}$$

$$\frac{d\Omega^*}{d\Omega} = P^3\left[P^{*2}\left(\overline{\gamma}\,P^* + \overline{\eta}\,E^*\cos\theta^*\right)\right]^{-1} \tag{15}$$

The counter telescope was mounted on a dolly and could be conveniently swung to any desired angle. The desired lab energy was obtained by varying the copper absorber placed between Counters 3 and 4 (see Fig. 6) and also that before Counter 3 for the high-energy pions. In order to minimize the effects of long-term drifts, data were taken many times in a cyclic procedure at each angle and energy setting. Target-full and target-empty runs were cycled regularly during the experiment.

Another computer program was used to calculate the copper absorber thickness for a given lab energy and the efficiency of the counter at that energy. In calculating the copper absorber thicknesses, energy losses in the liquid hydrogen, the aluminum cylinder, and the scintillation counters were also considered. The effective thicknesses of the absorbers were used in the calculations. Effective thickness includes an increase of thickness in the absorbers, since the pions in general do not pass through the counter telescope perpendicular to its axis. The Range-Energy Tables of Rich and Madey[21] were used, and an extrapolation between the given values was accomplished by using $T = aR^b$, where R is the range and a and b are constants determined by fitting the table values at the ends of the region.

The efficiency of the π^+ counter telescope is a product of three efficiencies: those taking account of (a) delay, (b) absorption, (c) multiple Coulomb scattering. The delay efficiency is the fraction of the π^+ mesons that decay into muons during the time when the muon pulses can make a coincidence with the gate. This fraction was measured experimentally and found to be 0.279. The absorption correction (2% to 40%) was calculated by using experimental cross sections.[22,23] The correction for multiple Coulomb scattering (6% and less), considering energy loss in the absorber, is described in the Appendix, page 52. Combining these three factors, we get the total efficiency, which is shown as the solid line in Fig. 9.

The two experimental points represent the number of π-μ telescope counts for an incident π^+ meson as measured in a "pure" π^+ beam. These points serve as a check on the delay and absorption efficiencies but contain the calculated multiple-scattering efficiency. The multiple-scattering correction was negligible in geometry used for the calibration run. The errors are a combination of counting statistics and uncertainty in beam contamination.

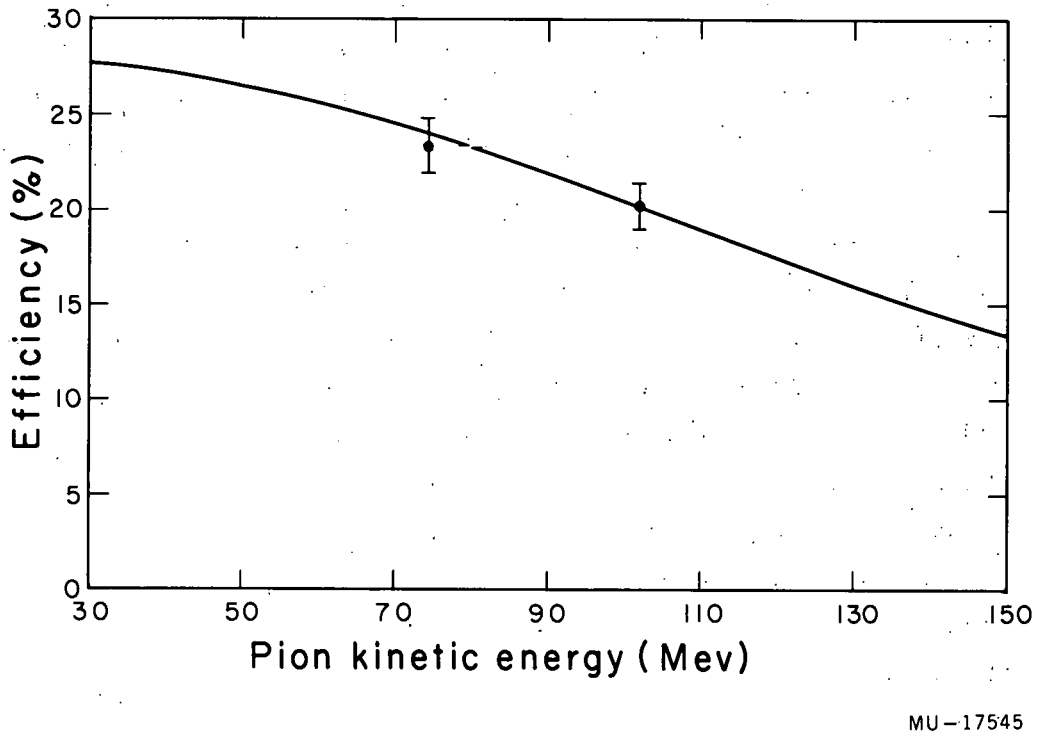

Fig. 9. Efficiency of π-μ telescope as a function of the kinetic energy of the stopping pion.

III. CORRECTIONS

Accidental counts in the π-μ telescope were monitored concurrently with the real counts. During the experiment the ratio of accidental to real counts was between 1/4 and 1.

Another correction had to be applied for "beam bunching." Because of the high-intensity π^- beams used, occasionally two pions bombarded the liquid hydrogen target during the same cyclotron fine-structure pulse. When this occurred, only one count was registered by the monitor counters, whereas each π^- meson was capable of producing a π^+ meson.

By delaying the signal in Counter 2 relative to Counter 1 by the separation between cyclotron fine-structure pulses, we measured the probability of two pions' passing through the monitor counters during adjacent fine-structure pulses. This was equal to the probability of two pions' passing through the monitor counters during the same fine-structure pulse. This probability had to be multiplied by the ratio of pions passing through the hydrogen target to those passing through the monitor counters, since only one π^- needed to pass through the monitor counters. Since all π^- mesons traversing the 2.25-in.-diameter collimator passed through Counter 1 and presumably the liquid hydrogen target, this ratio equalled the singles rate of Counter 1 divided by the doubles rate of Counters 1 and 2. This correction was directly proportional to beam intensity, and was $7 \pm 2\%$ or less for all intensities used.

The data analysis was complicated by the poor geometrical conditions used to obtain reasonable counting rates. Neglecting all other corrections for the time being, the problem is this: given $Y(\theta)$, the number of counts per incident π^- meson, with the counter at an angle θ as shown in Fig. 10, what is $\sigma(\theta)$, the differential cross section in the laboratory system? Let $L(\theta) = Y(\theta)/(nt)$, where nt is the number of hydrogen nuclei per cm^2 of target area.

The solution of a similar problem for a rectangular block target is presented by Anderson, Davidon, Glicksman, and Kruse.[24]

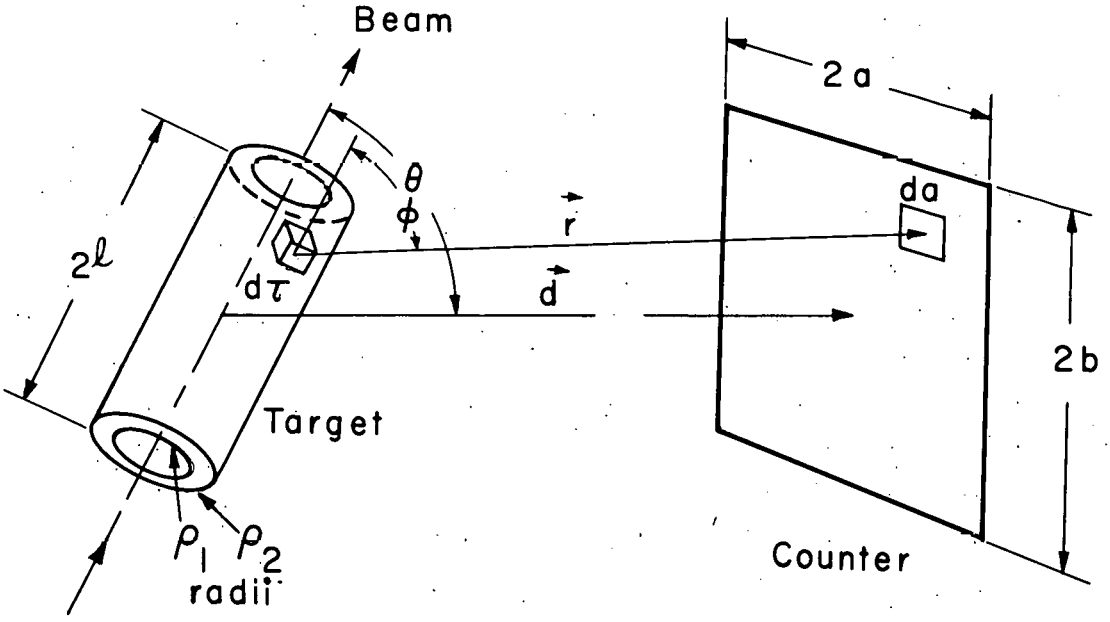

Fig. 10. Idealized target and counter geometry used as a basis for the geometric corrections.

If $\sigma(\phi)$ is the true differential cross section per hydrogen nucleus per unit solid angle for particles going from $d\tau$ to da, where $d\tau$ is an element of the target volume V, and da an element of the counter area A, we have

$$L(\theta) = \frac{1}{V} \int_V \int_A d\tau d\Omega \sigma(\phi).$$

The element of solid angle is

$$d\Omega = \frac{da}{r^2} \cos\delta,$$

where $\vec{r}$ is a vector connecting $d\tau$ with da, δ is the angle between $\vec{r}$ and the normal to the counter, and ϕ is the angle between $\vec{r}$ and the incident beam.

Expanding $\sigma(\phi)$ in a Taylor Series about $\phi = \theta$, we obtain

$$L(\theta) = \frac{1}{V} \int_V \int_A d\tau da \frac{\cos\delta}{r^2} \left[\sigma(\theta) + \sigma'(\theta)(\phi - \theta) + 1/2\ \sigma''(\theta)(\phi - \theta)^2\right].$$

For a counter of width 2a and height 2b at a distance d from the center of a target which is a hollow cylinder of length 2ℓ with inner and outer radii of ρ_1 and ρ_2 respectively, a long but straightforward calculation gives

$$\sigma(\theta) = L(\theta) \left\{(1+\alpha)\frac{A}{d^2}\left[1 + \frac{\beta}{1+\alpha}\frac{\sigma'(\theta)}{\sigma(\theta)} + \frac{\gamma}{1+\alpha}\frac{\sigma''(\theta)}{\sigma(\theta)}\right]\right\}^{-1}, \quad (16)$$

where (with $\mu = \cos\theta$) we have

$$\alpha = \frac{1}{2d^2}\left[-(a^2 + b^2) + \ell^2(3\mu^2 - 1) + 3/4\ R(1 - 3\mu^2)\right],$$

$$\beta = \frac{1}{6d^2}\left\{n\mu\left[a^2 + b^2 + 7\ell^2\sin^2\theta + 3/4\ R(7\mu^2 - 5)\right] - m\sin^2\theta\left[2(a^2 + \ell^2\sin^2\theta) + 3/2\ R\mu^2\right]\right\},$$

$$\gamma = \frac{n^2\sin^2\theta}{6d^2}\left[a^2 + \ell^2\sin^2\theta + 3/4\ R\mu^2\right],$$

$$n = 1 + 1/2\mu^2 + \frac{1\cdot 3}{2\cdot 4}\mu^4 + \frac{1\cdot 3\cdot 5}{2\cdot 4\cdot 6}\mu^6 + \cdots,$$

$$m = \mu \left[1/2 + \frac{1 \cdot 3}{2 \cdot 4} (2\mu^2) + \frac{1 \cdot 3 \cdot 5}{2 \cdot 4 \cdot 6} (3\mu^4) + \cdots \right],$$

and $\rho_1^2 + \rho_2^2$ has been replaced by

$$R = \frac{\sum_i N_i (\rho_{i+1}^2 + \rho_i^2)}{\sum_i N_i}$$

in the result in order to include N_i, the beam-particle density over the target volume. This calculation is accurate to second-order terms in a/d, ℓ/d, etc.

The $\sigma(\theta)$ in Eq (16) is calculated by an iteration process in which $L(\theta)$ is substituted for $\sigma(\theta)$ on the right side as a first guess.

For $\pi^- + p \rightarrow \pi^+ + \pi^- + n$ a three-body final state further complicated the determination of the second and third terms in Eq (16). However, rough estimates of $L'(\theta)$ and $L''(\theta)$ indicated that these terms were less than 3%, therefore they were neglected. The first factor a varied with angle from 0 to 7% in this experiment.

A correction was made for π^+ mesons decaying between the target and counter telescope. The magnitude of this correction varied from 2% to 6%, depending on the π^+ meson's kinetic energy.

IV. RESULTS

Measurements were taken for π^+ mesons emitted at 60°, 90°, 125°, and 160° in the barycentric system for incident π^- kinetic energies of 317, 371, and 427 Mev. For a π^- kinetic energy of 260 Mev only a single measurement was made at 90° in the laboratory system. For each angle, measurements were made for one or more π^+ energies. The differential cross section as a function of π^+ angle and kinetic energy is related to the experimental data by the formula

$$\frac{d^2\sigma}{d\Omega^* dT^*} = Y(\theta, T)\left[nt(1+\alpha)\frac{A}{d^2}\eta(1-\epsilon)\frac{d\Omega^*}{d\Omega}\Delta T^*\right]^{-1}.$$

Here $Y(\theta, T)$ is the net number of π^+ mesons (target full minus target empty) counted per incident π^- meson. This has been corrected for accidentals and beam bunching. The quantity nt is the number of hydrogen nuclei per cm^2 of target area. The mean target thickness was 4.320 in., and the difference in density between liquid hydrogen and hydrogen gas was determined[25] as 0.069 g/cm^3, resulting in $nt = 4.565 \times 10^{23}$ nuclei/cm^2. The term $(1+\alpha)\frac{A}{d^2}$ is the effective solid angle subtended by the counter telescope, $\frac{A}{d^2}$ in the laboratory system; η is the efficiency of the counter telescope (see Fig. 9); ϵ is the fraction of the pions that decay between the hydrogen target and the counter telescope; $\frac{d\Omega^*}{d\Omega^*}$ is solid-angle transformation from the barycentric to the laboratory system, and is given by Eq (15); ΔT^* is the energy-acceptance band in the c.m. system for Counter 4.

The experimental results for $\frac{d^2\sigma}{d\Omega^* dT^*}$ are presented in Table II. Curves of $\frac{d^2\sigma}{d\Omega^* dT^*}$ versus T^* are shown in Figs. 11 through 15. The solid line is the relativistic phase-space curve as given by Block.[26] The heights of the phase-space curves were determined by minimizing the weighted sum of the squares of the differences between the calculated and experimental values.

The statistical phase-space curves fit the data adequately for incident energies of 317 and 427 Mev, but the phase-space

Table II

Differential cross section with respect to π^+ angle and energy

	θ^* (deg)	T^* (Mev)	ΔT^* (Mev)	$\frac{d^2\sigma}{d\Omega^* dT^*}$ (μb/sterad-Mev)
T_l = 260 Mev, T^*_{max} = 57.1 Mev	115.2	45.4	21.4	0.21 ± .11
	63.0	36.7	11.8	0.846± .31
	90.0	28.6	16.1	0.853± .19
T_l = 317 Mev, T^*_{max} = 91.3 Mev	91.3	48.3	14.9	0.794± .20
	89.3	62.1	13.1	0.770± .24
	125.1	52.9	23.5	0.592± .15
	122.6	73.6	18.5	0.447± .24
	158.5	73.3	32.9	0.745± .18
	59.7	40.9	10.5	2.05 ± .46
	60.0	74.3	10.3	1.21 ± .27
	60.1	103.6	9.5	0.59 ± .35
T_l = 371 Mev, T^*_{max} = 122.1 Mev	92.1	34.5	15.5	1.98 ± .33
	90.0	57.9	13.4	1.55 ± .40
	90.1	78.8	12.4	0.91 ± .29
	90.1	104.3	12.4	0.88 ± .24
	127.2	55.4	23.9	1.77 ± .27
	124.5	76.4	18.8	1.32 ± .43
	125.1	103.3	17.6	0.93 ± .24
	159.3	77.9	34.1	1.38 ± .25
	160.0	109.0	26.0	0.42 ± .30
	60.6	43.0	10.0	2.88 ± .45
	60.3	88.9	9.5	2.93 ± .50
T_l = 427 Mev, T^*_{max} = 152.6 Mev	90.3	45.0	13.4	2.17 ± .48
	90.3	90.0	12.0	2.61 ± .53
	90.4	124.5	11.6	1.01 ± .42
	125.3	57.6	23.7	1.55 ± .32
	125.3	111.4	17.0	1.26 ± .26
	160.2	82.6	37.0	1.65 ± .39

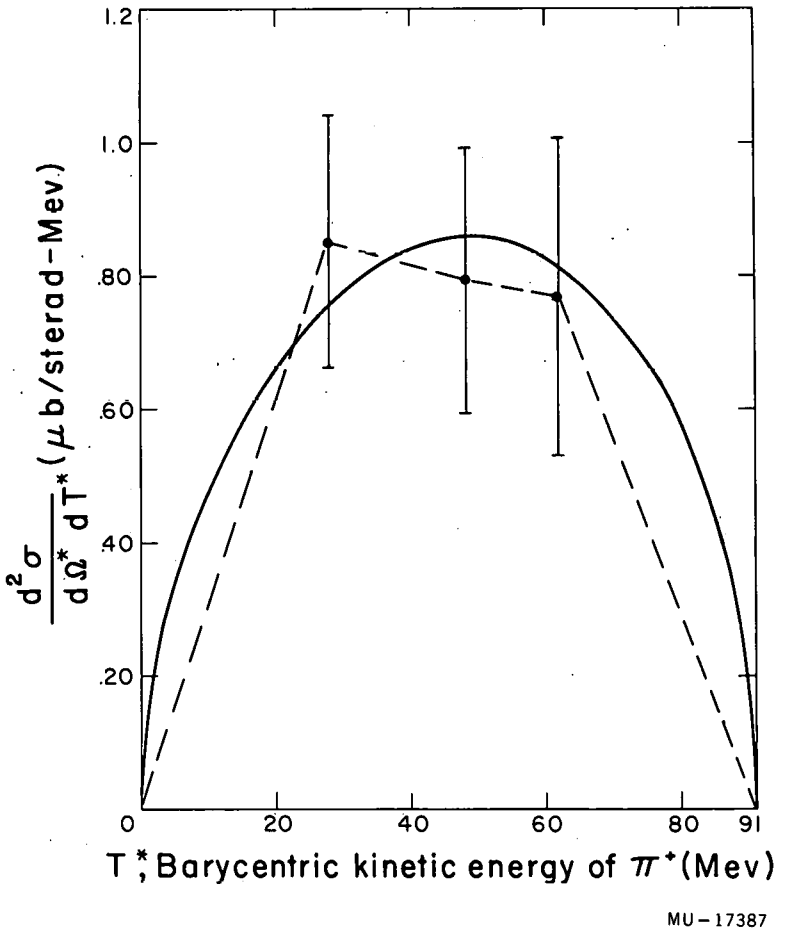

Fig. 11. Differential cross section for $\pi^- + p \rightarrow \pi^+ + \pi^- + n$ as a function of π^+ kinetic energy for incident π^- kinetic energy of 317 Mev and π^+ barycentric angle of 90°.

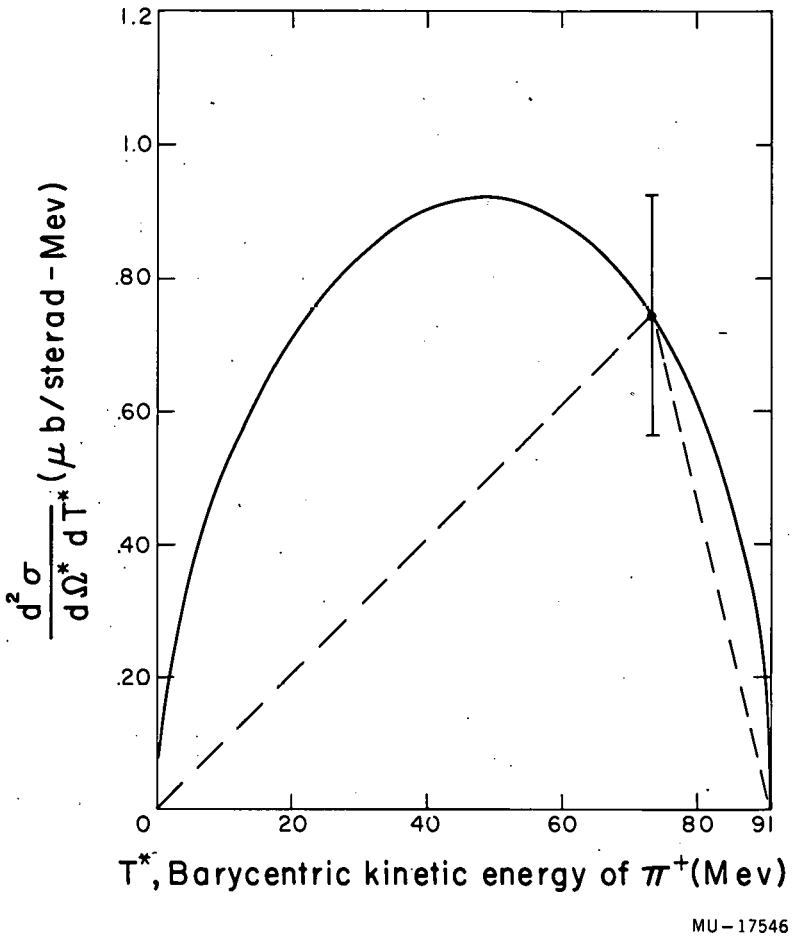

Fig. 12. Differential cross section for $\pi^- + p \rightarrow \pi^+ + \pi^- + n$ as a function of π^+ kinetic energy for incident π^- kinetic energy of 317 Mev and π^+ barycentric angle of 159°.

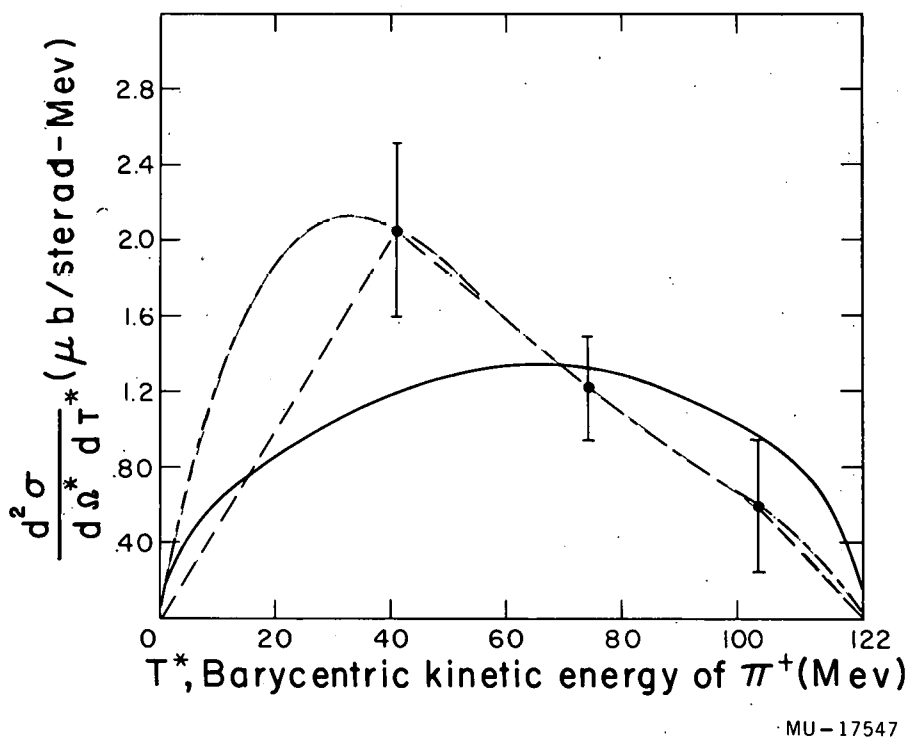

Fig. 13. Differential cross section for $\pi^- + p \rightarrow \pi^+ + \pi^- + n$ as a function of π^+ kinetic energy for incident π^- kinetic energy of 371 Mev and π^+ barycentric angle of 60°.

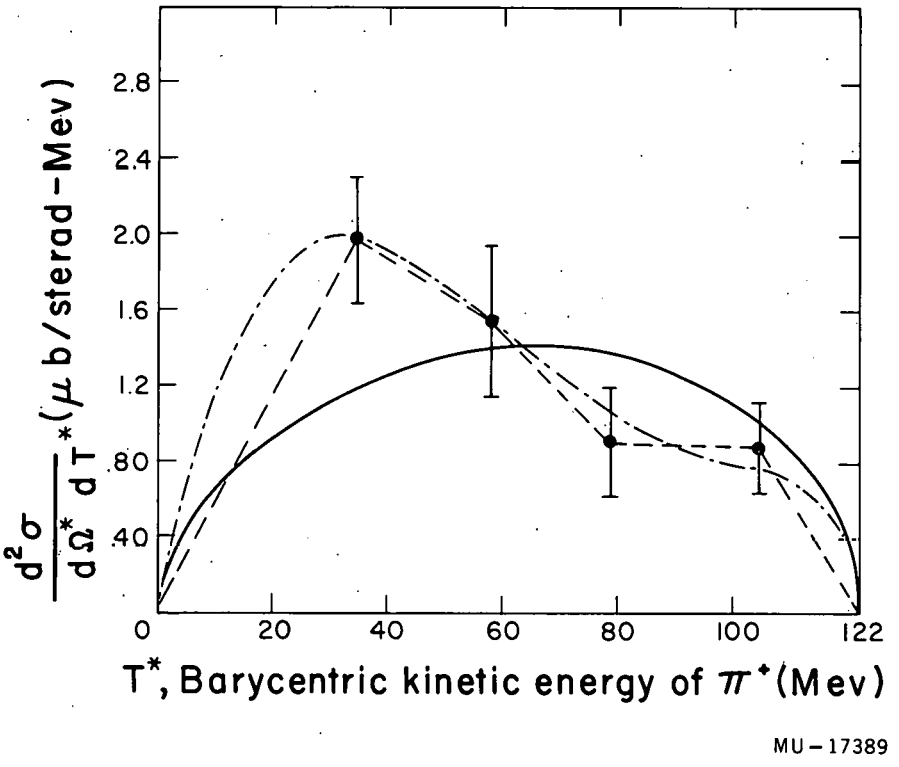

Fig. 14. Differential cross section for $\pi^- + p \rightarrow \pi^+ + \pi^- + n$ as a function of π^+ kinetic energy for incident π^- kinetic energy of 371 Mev and π^+ barycentric angle of 90°.

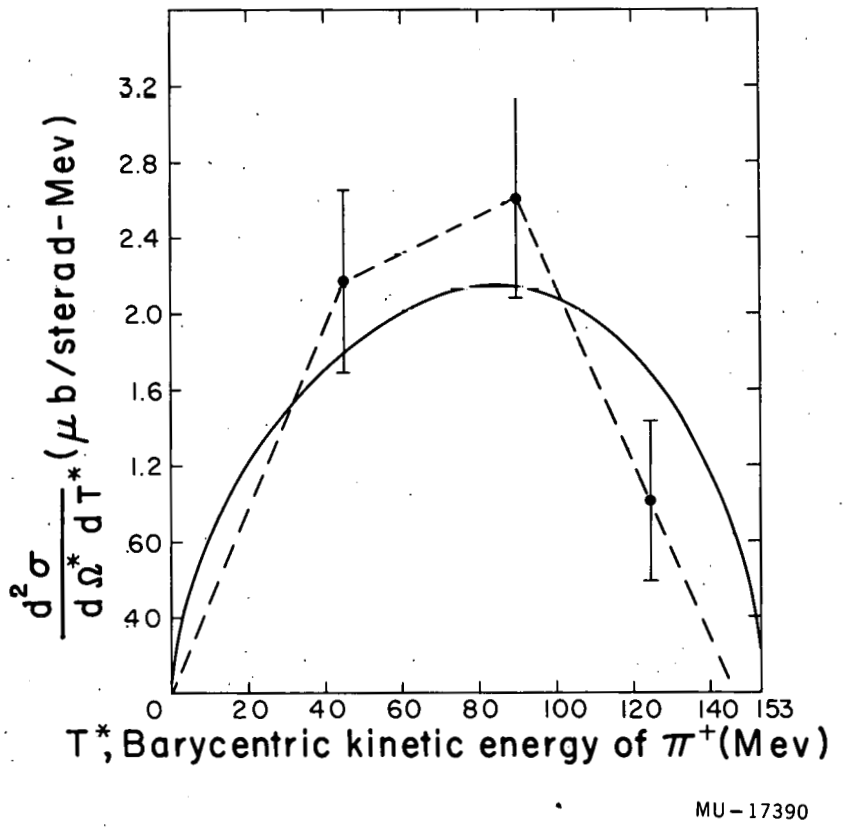

Fig. 15. Differential cross section for $\pi^- + p \rightarrow \pi^+ + \pi^- + n$ as a function of π^+ kinetic energy for incident π^- kinetic energy of 427 Mev and π^+ barycentric angle of 90°.

calculation predicts too few low-energy π^+ mesons at 371 Mev. To obtain the angular differential cross section an integration was performed over the energy of the π^+ meson. The phase-space curves (solid lines) were used for 317 and 427 Mev, while the dash-dot curves were used for 371 Mev. The dashed curves were used to estimate a lower limit for the total cross sections.

Table III gives $\frac{d\sigma}{d\Omega^*}$ resulting from the integration. The errors listed are statistical only and do not include the errors involved in integration over energy.

Table III

Differential cross section with respect to π^+ angle

T_1 (Mev)	θ^* (deg)	$d\sigma / d\Omega^*$ (μbarn/sterad)
317	63	62 ± 23
317	90	60.2 ± 9
317	124	41.0 ± 9
317	159	64.4 ± 16
371	60	154 ± 19
371	90	152 ± 18
371	125	165 ± 20
371	160	145 ± 26
427	60	369 ± 42
427	90	245 ± 35
427	125	173 ± 25
427	160	189 ± 45

The angular differential cross sections as a function of the barycentric angle of the π^+ meson are shown in Figs. 16 through 18. Least-squares fits to the experimental points were made by assuming a polynomial in cos θ^*. The curve of the form $\frac{d\sigma}{d\Omega^*} = a_o + a_1 \cos\theta^*$ is shown as the solid line in Figs. 16-18. At 317 and 371 Mev a curve of the form $\frac{d\sigma}{d\Omega^*} = a_o$ would also fit the data. The Russian data by Zinov and Korenchenko[12] -- shown for comparison only and not used in the least-squares fitting -- was obtained with counters in a quite different manner. The π^+ and π^- from $\pi^- + p \rightarrow \pi^+ + \pi^- + n$ and 70% of the π^- mesons from $\pi^- + p \rightarrow \pi^- + \pi^o + p$ were counted for $\theta^* = 106^o$ and $T^* \geq T^*_{max}/2$. To obtain the plotted points, it was assumed that the cross sections for both reactions were equal and $\frac{d^2\sigma}{d\Omega^* dT^*}$ was symmetrical about $T^* = T^*_{max}/2$. The assumption of equal cross sections is not critical, as the ratio of detection efficiencies for $\pi^- + p \rightarrow \pi^+ + \pi^- + n$ to $\pi^- + p \rightarrow \pi^- + \pi^o + n$ is 2/0.7. When one considers the assumptions involved, the agreement is quite good.

Another integration was performed to obtain the total cross sections. For 260 Mev an isotropic differential cross section was assumed. The results are listed in Table IV with the experimental errors representing the combined errors of counting statistics and integration over angle and energy.

Table IV

Total cross sections for $\pi^- + p \rightarrow \pi^+ + \pi^- + n$

T_l (Mev)	σ (mb)
260	0.14 ± 0.10
317	0.71 ± 0.17
371	1.93 ± 0.37
427	3.36 ± 0.74

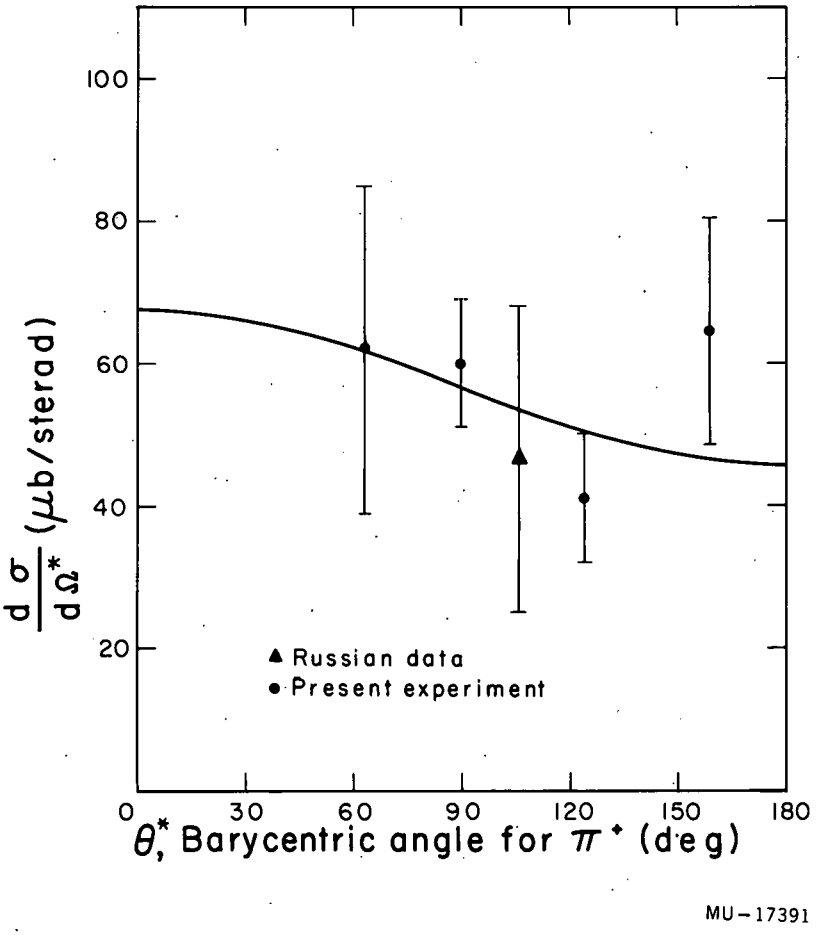

Fig. 16. Angular differential cross section for π^+ meson for an incident π^- meson of 317 Mev.

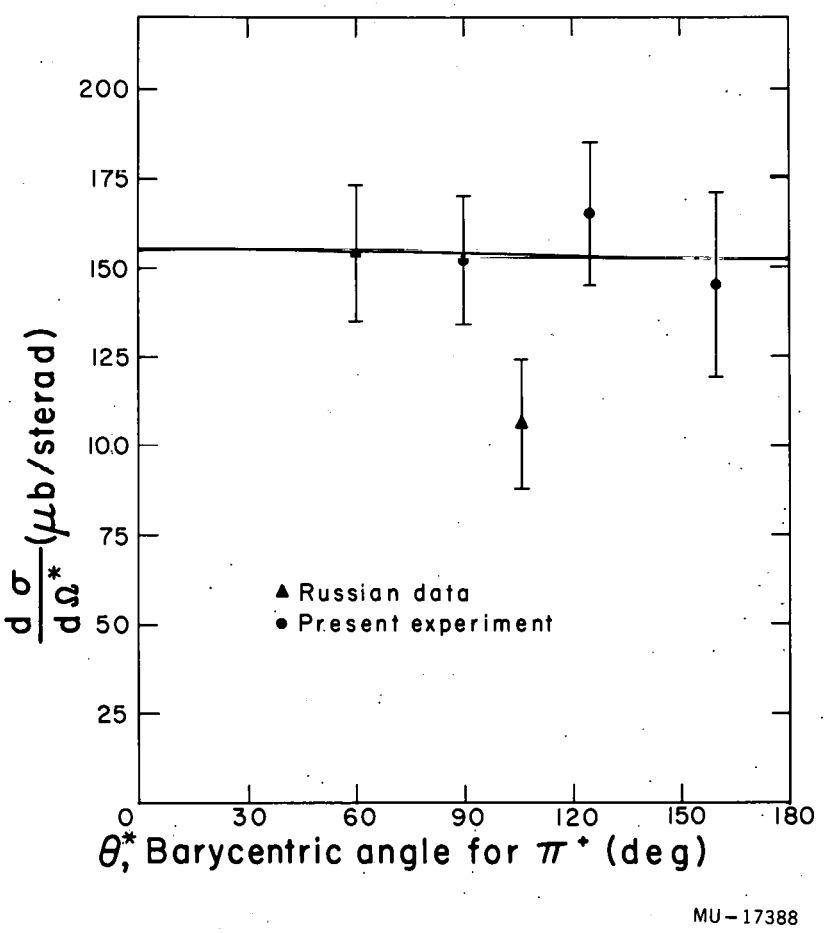

Fig. 17. Angular differential cross section for π^+ meson for an incident π^- meson of 371 Mev.

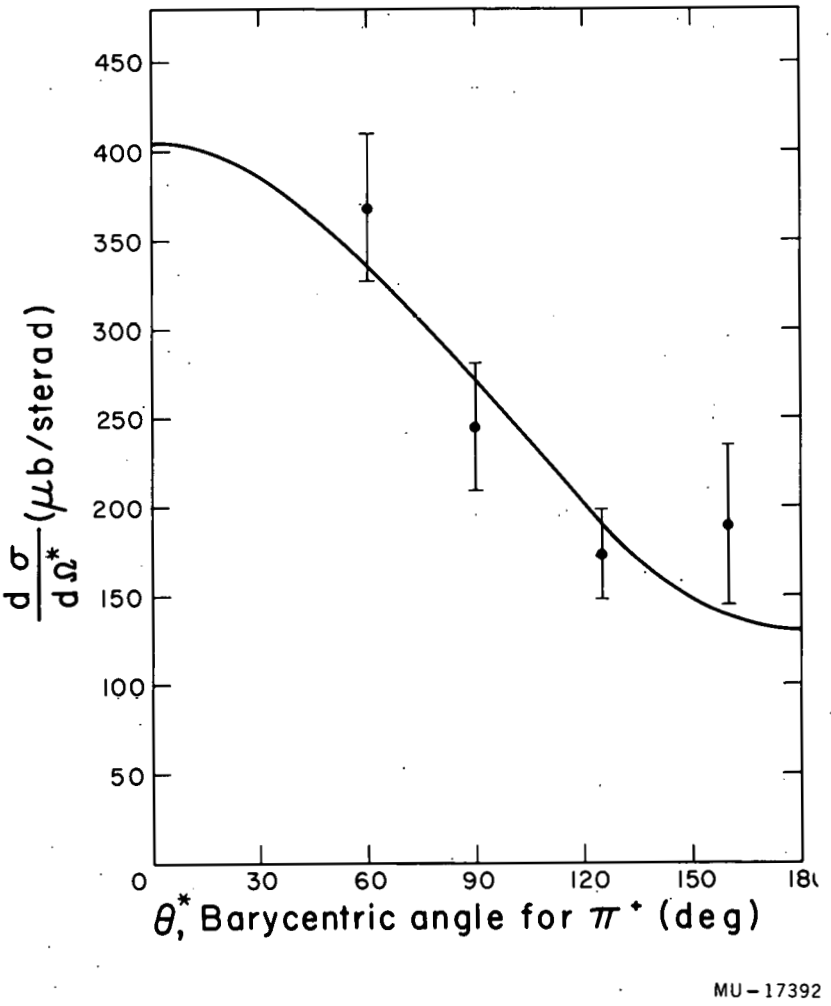

Fig. 18. Angular differential cross section for π^+ meson for an incident π^- meson of 427 Mev.

A curve of the total cross section as a function of the incident π^- kinetic energy is shown in Fig. 19. The solid line and dashed line are theoretical curves and are discussed in Section V. Since the theoretical predictions are much lower than the experimental result, it is important to obtain an experimental lower limit including all errors. The error due to uncertainty in the efficiency of the π-μ counter telescope was estimated to be 6%. This and the smaller errors due to uncertainty in beam contamination and other corrections were negligible in comparison with the statistical errors and the uncertainty in the shape of π^+-meson energy spectrum. By using the dashed-lined curves shown in Figs. 11-15, and folding in the statistical error, we obtain the standard deviations given in Table IV.

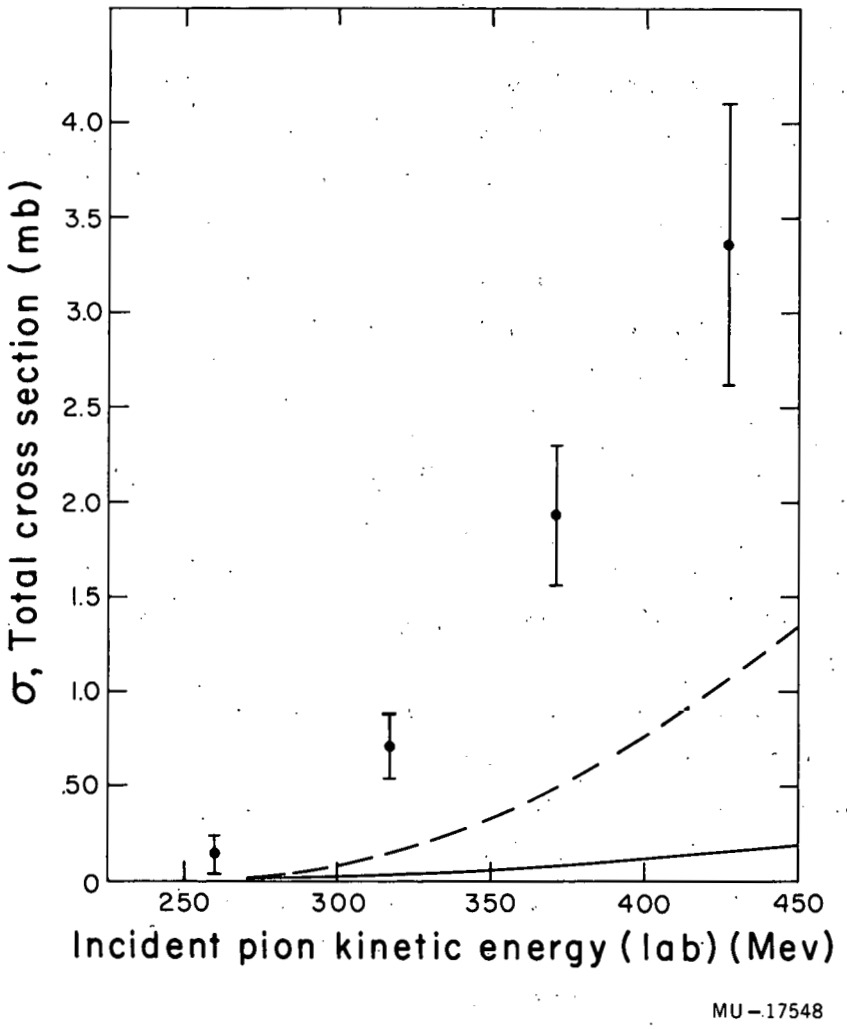

Fig. 19. Total cross section for $\pi^- + p \rightarrow \pi^+ + \pi^- + n$ as a function of the π^- kinetic energy (lab). The curves are the theoretical predictions based on the static model. The solid curve is prediction by Kazes[16] while the dashed curve is the prediction by Franklin.[14]

V. DISCUSSION

The dashed line in Fig. 19 is the theoretical prediction given by Franklin.[14] The solid line is the theoretical prediction by Kazes;[16] Rodberg's prediction for this cross section is even smaller.[15] All these predictions are based on the static model, and the variation in the result is caused by the different approximations used. Because of his use of the Born approximation, Franklin's earlier results do not obey unitarity in the one-meson approximation. The results of Rodberg and Kazes obey unitarity in the one-meson approximation and therefore are probably a more accurate interpretation of the static-model prediction.

This means that the systematic discrepancy between this theory and experiment is not a factor of three[14] but a factor of ten.[15, 16] The effect of including nucleon recoil in the calculations of the total cross sections is believed to be too small in this energy region to account for this large a discrepancy.[27]

The existence of a pion-pion interaction has been postulated to explain the nucleon structure[28] and the peak[29-31] in the π^--proton total cross section near 1 Bev. The direct interaction of the incident pion and a virtual pion in the meson cloud surrounding the nucleon could contribute significantly to the production of a secondary pion in pion-nucleon collisions. The effect of a pion-pion interaction on the production cross section is discussed by Barshay[32] and more specifically by Rodberg[33] in connection with the particular reaction under study here. The solid line in Fig. 20 shows a fit to the experimental data by Rodberg[33] corresponding to physically plausible pion-pion phase shifts.

At very high incident energies, at which the momentum of the virtual pion is much less important, the energy and angular distributions predicted by the π-π interaction model are these: (a) the pions in the final state should be in the high-energy region of their available phase space and go forward in the π^- - p center-of-mass system, (b) the nucleon should act as a spectator and receive only

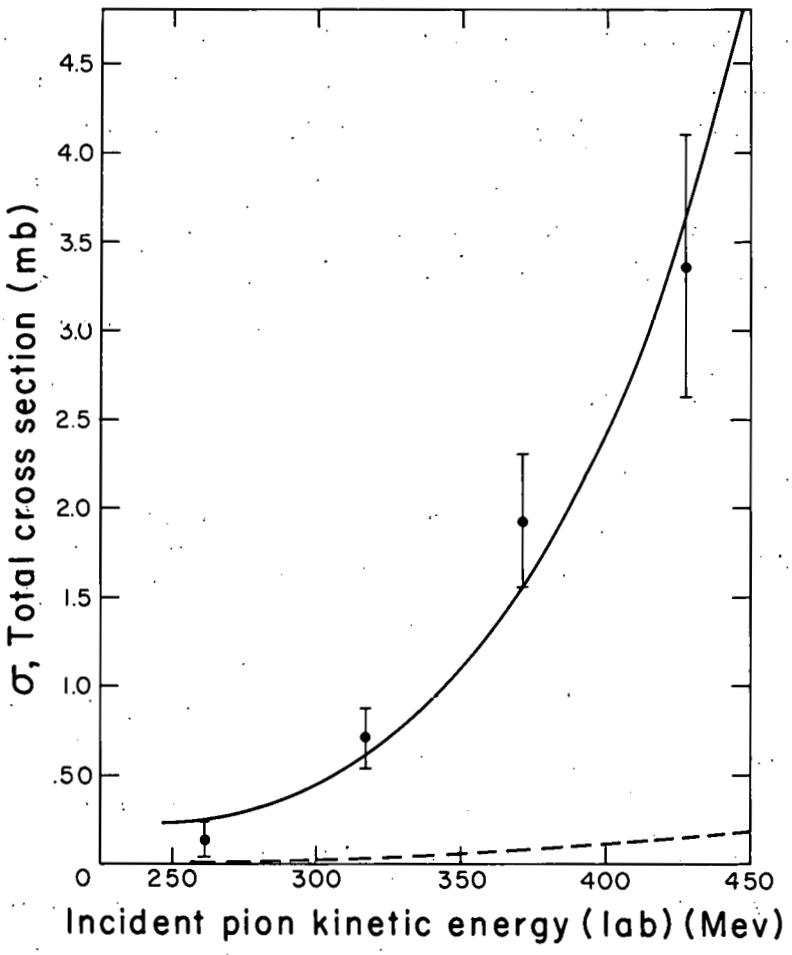

Fig. 20. Total cross section for $\pi^- + p \rightarrow \pi^+ + \pi^- + n$ as a function of the π^- kinetic energy (lab). Solid curve is the theoretical results from Rodberg[33] based on pion-pion interaction model. Dashed curve is the theoretical prediction based on the static model by Kazes.[16]

a small recoil momentum and go backward in the c.m. system. At 4.5 Bev the general features of effects (a) and (b) have been observed.[5] For low incident-pion energies, the momentum of the virtual pion tends to obscure these effects and the nucleon receives a momentum comparable to that of the incident pion.

At the energies of this experiment it is not possible to differentiate between the pion-pion interaction model and the static model on the basis of π^+ energy spectrum.

The angular differential cross sections (see Figs. 16-18) are nearly isotropic at 317 and 371 Mev, but peaked forward at 427 Mev. Apparently the fore-aft asymmetry predicted at high energies[33] is washed out at the lower energies of 317 and 371 Mev, but appears at the higher energy of 427 Mev.

Our results combined with those obtained by Zinov and Korenchenko[12] indicate that the ratio $\frac{\pi^- + p \rightarrow \pi^+ + \pi^- + n}{\pi^- + p \rightarrow \pi^- + \pi^0 + p}$ is probably 1 or greater. At 810 Mev the measured ratio[10] is 2.49. The static model[14,16] predicts that the ratio should be about 1/3, while the pion-pion interaction model[30,33] predicts about 2/1, which is in better agreement with the experimental results.

The observed total cross sections for $\pi^- + p \rightarrow \pi^+ + \pi^- + n$ indicate much larger cross sections than the theoretical prediction based on the static model. Reasonable agreement with experiment can be obtained by the inclusion of a pion-pion interaction in the production mechanism.

ACKNOWLEDGMENTS

I am indebted to Professor A. C. Helmholz for his guidance and encouragement throughout my graduate work. Thanks are also due Drs. Robert Kenney and Victor Perez-Mendez for their helpful advice and assistance during this experiment. Special mention is also due Mr. John Caris for his generous help throughout the entire experimental program. I would also like to acknowledge the help of Dr. Edward Knapp and Mr. Lester Goodwin.

Finally, I wish to thank Mr. James Vale and the cyclotron crew for their assistance and cooperation during the course of the experimental work.

This work was done under the auspices of the U.S. Atomic Energy Commission.

APPENDIX

Counter Telescope Calibration

A similar calibration of a π-μ telescope was performed by Knapp.[34] The only essential difference is that with his counter telescope the geometry was such that multiple Coulomb scattering could be neglected. Here multiple scattering had to be considered and a calculation was made.

The experimental arrangement used for the calibration is shown in Fig. 21. Here the wedge magnet was used to obtain a nearly monocnergetic beam. The magnet was actually defocusing the particles, but a high flux was not needed for the calibration.

Positive pion beams of kinetic energy 74 and 102 Mev were used. Integral and differential range curves for the 102-Mev beam are shown in Figs. 22 and 23 respectively. For the integral range curve in Fig. 22, A is the break between the pion absorption-loss curve and the stopping of the pions, B is the break between the pions and the muons (these are the same as A and B for the 371-Mev π^- integral range curve, Fig. 3), and C is the break between the muons and electrons. The muon contamination was estimated, by subtracting the ordinate at C from the ordinate at B, to be 12.5±2.0%. The fraction of muons lost by multiple Coulomb scattering was negligible.

The electron contamination measured at C represents the fraction of the electrons left after attenuation in 62.5 g/cm^2 Cu and must be extrapolated to zero copper. Electron range curves, taken at the synchrotron[35] for electrons of approximately the same momentum as the pion beams, were used to facilitate the extrapolation. The extrapolation indicated an electron contamination of 10±3%.

The electronics used for the range curves is shown in Fig. 24. Counters 1 and 2 were the same as those used for monitoring the negative pion beam. Counter 6 was a 6-in.-diameter disk, 0.5 in. thick, and Counter 7, an anticoincidence counter, was a 12-in.-diameter disk 1 in. thick. In Fig. 22 "Triples/doubles" represents

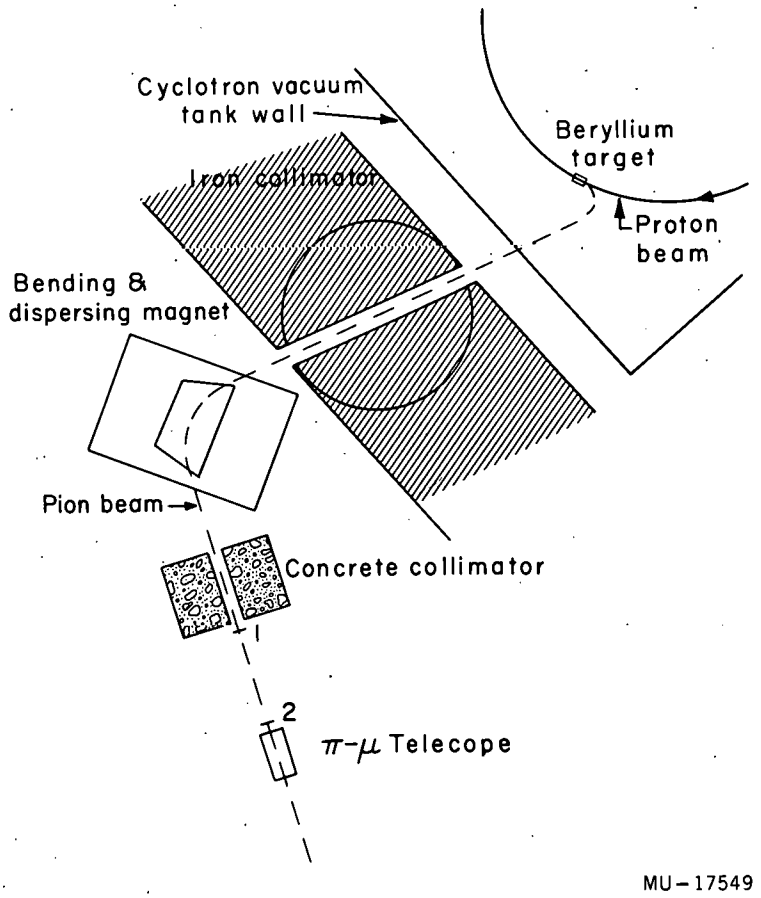

Fig. 21. Experimental arrangement for calibration of π-μ telescope with positive pion beam.

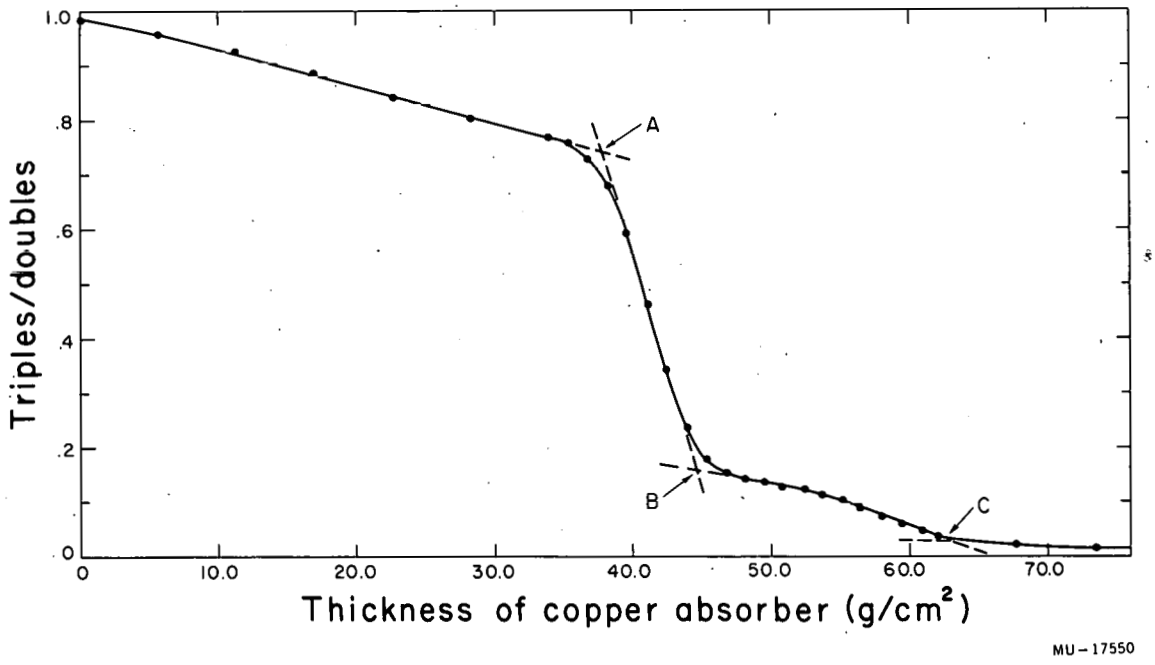

Fig. 22. Integral range curve for 102-Mev positive pion beam.

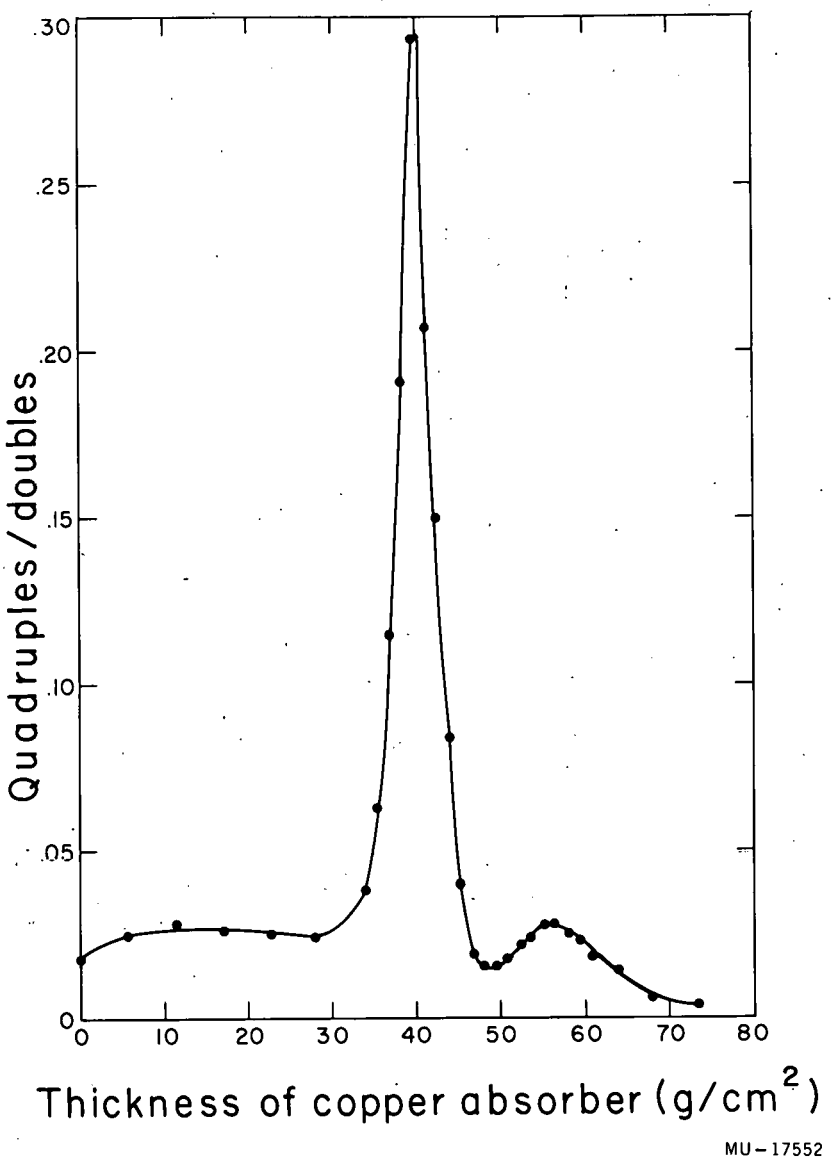

Fig. 23. Differential range curve for 102-Mev positive pion beam.

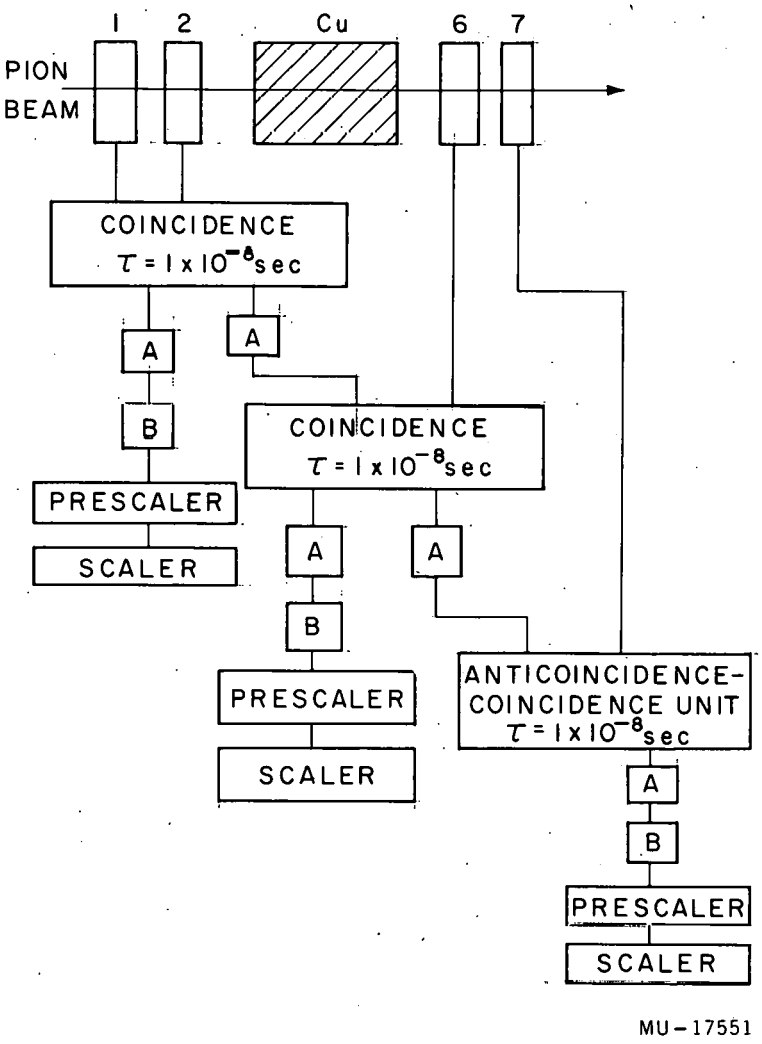

Fig. 24. Block diagram of electronics used for integral and differential range curves.

the ratio of coincidences 1+2+6 to coincidences 1+2. In Fig. 23 "Quadruples/doubles" represents the ratio of coincidences 1+2+6-7 to coincidences 1+2. The electronics used for the calibration of the π-μ counter telescope is identical with that shown in Fig. 7 except now π^+ mesons pass through Counters 1 and 2.

During the calibration run a plateau in the meson counting rate as a function of the high voltage was observed for each counter. A typical plateau curve is shown in Fig. 25. The proper delay settings were made by observing the counting rate as a function of the delay of one or two counters relative to all others. The delay curve in Fig. 26 was obtained by changing the length of RG-63/U cable between the monitor counters and the counter telescope.

By varying the delay of the gate relative to Counter 4 the mean-life curve shown in Fig. 27 was obtained. From this curve the delay efficiency was determined. When this curve was taken the Cu absorber was adjusted so that a reasonable number of pions would stop in Counter 4 but the electrons and muons would pass through into Counter 5, which was in anticoincidence. As the gate delay is decreased, eventually a point is reached at which the incident-pion pulse will make a coincidence with the gate; this is the flat region in Fig. 27. As only pions stop in Counter 4 and the anticoincidence rejects the muons and electrons, the delay efficiency is the ratio of the counting rate at the operating point to the counting rate in the flat region where all stopping pions are counted.

The correction for multiple Coulomb scattering was based on the geometrical calculations of Sternheimer[36], but included the energy-loss considerations of Eyges[37]. It was assumed that in the absence of any absorber the incident π^+-meson beam emerging from the hydrogen target was uniformly distributed over the surface of Counter 4. Also it was assumed that the pion beam's direction was parallel to the axis of counter telescope as shown in the following figure.

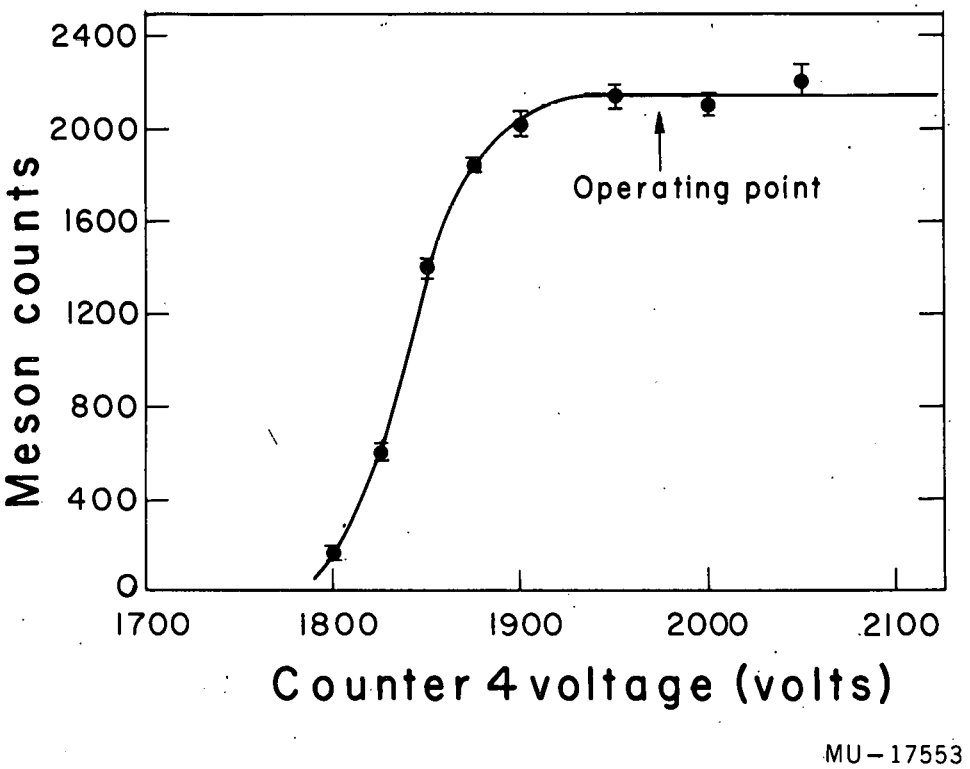

Fig. 25. High-voltage plateau curve of Counter 4.

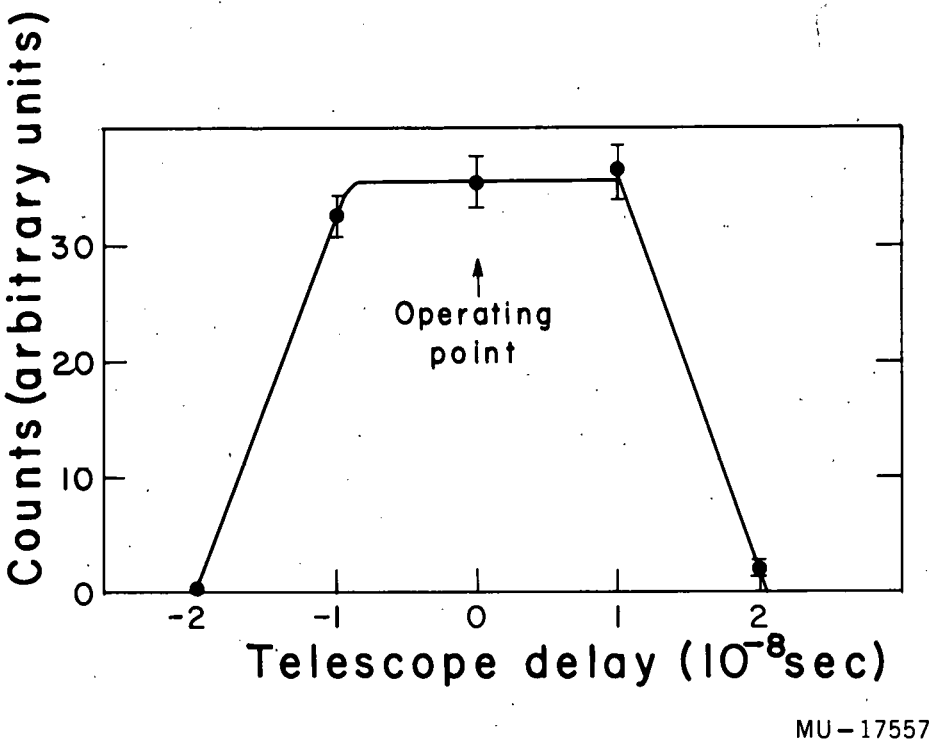

Fig. 26. Delay curve between monitor counters and π-μ counter telescope.

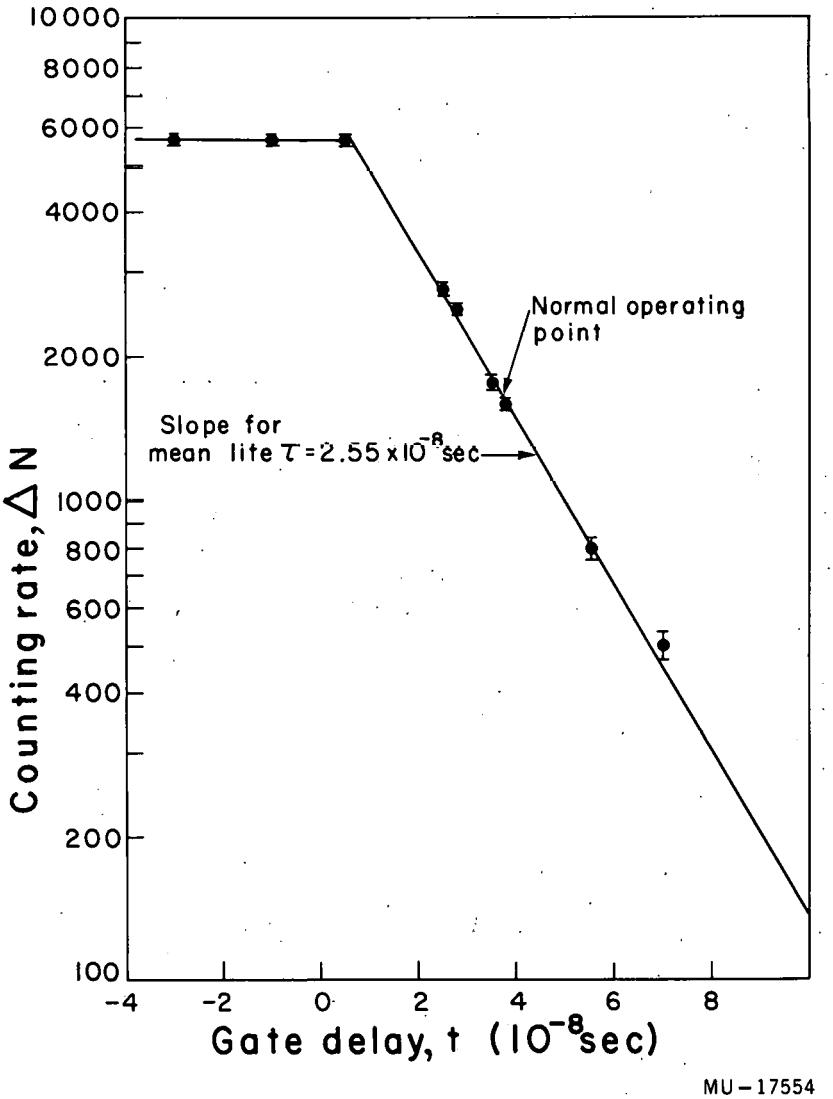

Fig. 27. Differential mean-life curve for particles counted in positive pion beam. Straight line is for $\Delta N = \frac{N_o \Delta t}{\tau} e^{-t/\tau}$ with $\tau = 2.55 \times 10^{-8}$ sec.

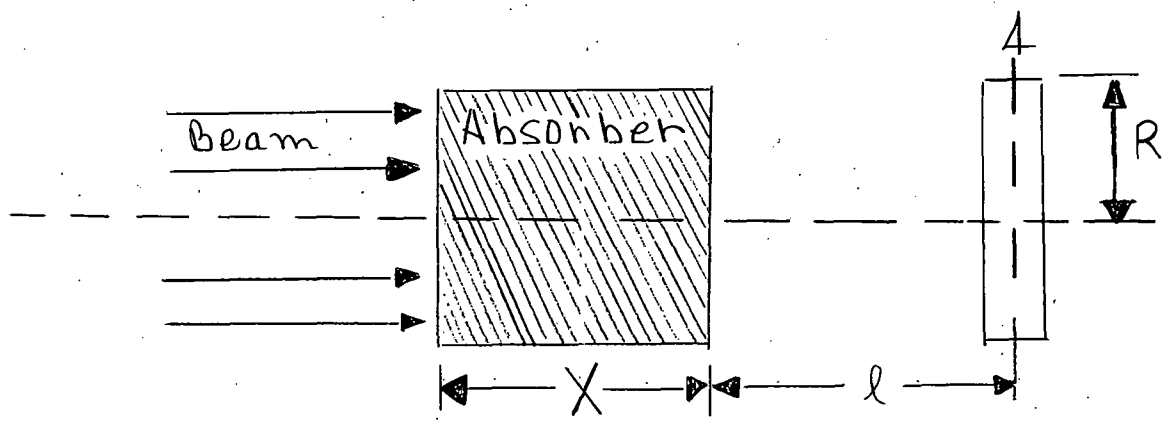

For a parallel, uniform beam of radius ρ_o passing through an absorber of thickness x at a distance ℓ from a counter of radius R, the fraction of the beam that strikes the counter is $F(r'_o, \rho'_o)$. F is a function of only $\rho'_o = \rho_o/R$ and the quantity

$$r'^2_o = \frac{E_s^2}{R^2 X_o} \int_o^x \frac{(\ell + x - \eta)^2}{(\beta P)^2} \, d\eta, \qquad (17)$$

where $E_s = 21$ Mev, β and P are the velocity and momentum of the particle, respectively, and X_o is the radiation length for the absorber in g/cm^2; R, ℓ, x, η are in units of g/cm^2 of the absorber. Equation (17), which corresponds to Eyges' equation[37] (13c), was integrated numerically by using range-energy tables to determine the particles' energy after traversing an absorber of thickness η.

Using r'_o thus obtained, we read $F(r'_o, \rho'_o)$ directly from a graph given by Sternheimer.[36] This correction (1-F) turned out to be small--6% or less for the copper absorber thicknesses used during the experiment.

The absorption loss was calculated by

$$\eta \text{ abs} = \exp\left[\frac{-nt}{T_f - T_i} \int_{T_i}^{T_f} \sigma(T) \, dT\right],$$

where nt is the number of nuclei/cm^2 in the absorber, T_i and T_f are the initial and final energies of the pions, and $\sigma(T)$ is the

absorption cross section as a function of the pions' energy obtained from the experimental values.[22,23]

Using the calculated absorption and multiple Coulomb scattering losses and the measured delay efficiency, we obtained the solid line of Fig. 9. This is in good agreement with the two experimental points obtained by the other method described below.

Another method was used in which the product of the delay efficiency times the absorption efficiency was measured. This consisted in measuring the ratio of pions counted by the π-μ telescope to those counted by the monitor. Since not quite all the pions stopped in Counter 4, because the energy spread of the beam was greater than that accepted by the counter, it was necessary to vary the thickness of copper absorber between Counters 3 and 4 to take account of these high- and low-energy pions.

Figure 28 is the curve of the π-μ counting rate versus the copper absorber thickness. The dashed line shows the equivalent copper absorber thickness of Counter 4. The sum of the solid-curve values at the center of the three histograms gave the number of π-μ counts. The incident beam was corrected for contamination and we obtained the desired ratio of π-μ counts to incident pions. The experimental points in Fig. 9 were obtained in this manner. In the geometry used for the calibration, the beam is defined by a 2-in.-diameter counter located 5 in. before the π-μ telescope. The correction for multiple Coulomb scattering for this geometrical arrangement was shown by calculation to be negligible.

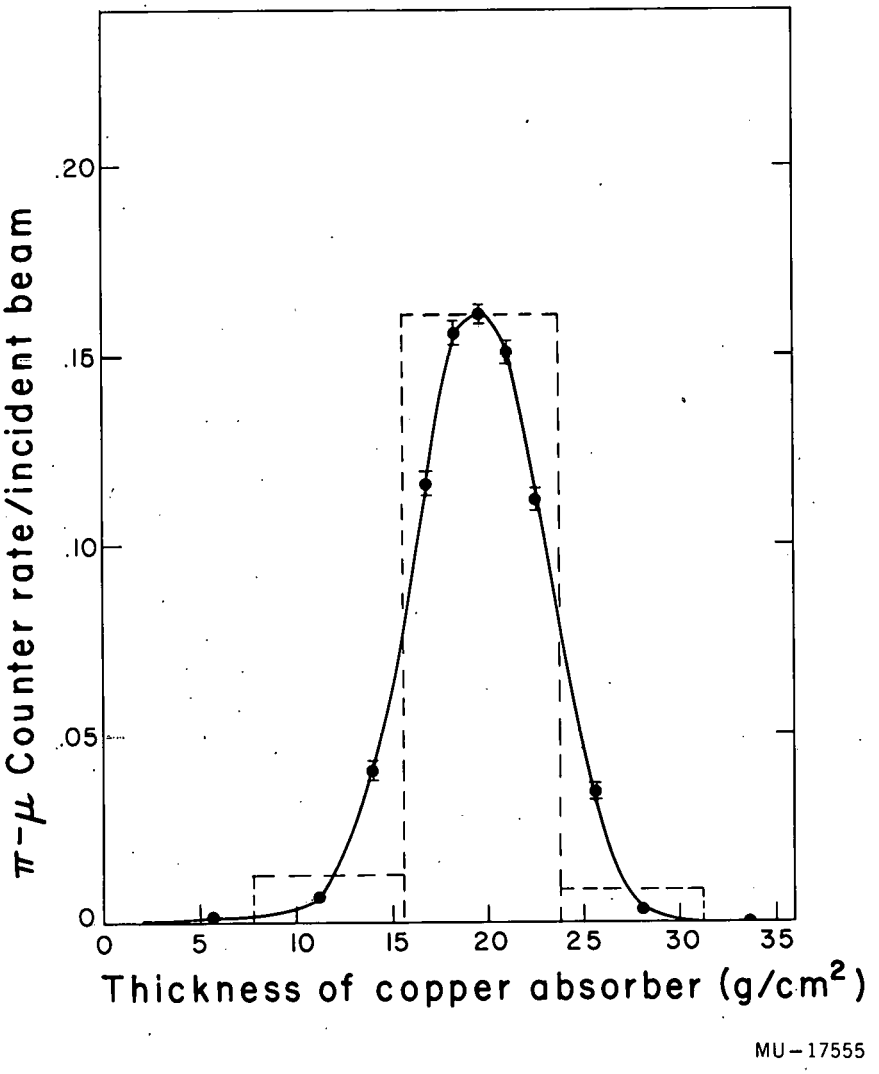

Fig. 28. Calibration curve for π-μ counter telescope.

REFERENCES

1. J. Crussard, W. D. Walker, and M. Koshiba, Phys. Rev. 94, 736 (1954).
2. M. Blau and M. Caulton, Phys. Rev. 96, 150 (1954).
3. W. D. Walker and J. Crussard, Phys. Rev. 98, 1416 (1955).
4. W. D. Walker, F. Hushfar, and W. D. Shephard, Phys. Rev. 104, 526 (1956).
5. W. D. Walker, Phys. Rev. 108, 872 (1957).
6. L. M. Eisberg, W. B. Fowler, R. M. Lea, W. D. Shephard, R. P. Shutt, A. M. Thorndike, and W. L. Whittemore, Phys. Rev. 97. 797 (1955).
7. G. Maenchen, W. F. Fowler, W. M. Powell, and R. W. Wright, Phys. Rev. 108, 850 (1957).
8. M. E. Blevins, M. M. Block, and J. Leitner, Phys. Rev. 112, 1287 (1958).
9. A. R. Erwin and J. K. Kopp, Phys. Rev. 109, 1364 (1958).
10. L. Baggett, π^--p Elastic Scattering and Single Pion Production at 0.939 Bev/c, UCRL-8302, May 1958.
11. R. R. Crittenden, J. H. Scandrett, W. D. Shephard, W. D. Walker, and J. Ballam, Phys. Rev. Lett. 2, 121 (1959).
12. V. G. Zinov and S. M. Korenchenko, Zhur. Eksptl. i Teoret. Fiz. 34, 301 (1958) [Translation: Soviet Phys. JETP 34(7), 210 (1958)].
13. S. Barshay, Phys. Rev. 103, 1102 (1956).
14. J. Franklin, Phys. Rev. 105, 1101 (1957).
15. L. S. Rodberg, Phys. Rev. 106. 1090 (1957).
16. E. Kazes, Phys. Rev. 107. 1131 (1957).
17. W. G. Cross, Rev. Sci. Instr. 22, 717 (1951).
18. F. Evans, UCRL Counting Handbook (unpublished).
19. O. Chamberlain, R. F. Mozley, J. Steinberger, and C. Wiegand, Phys. Rev. 79, 394 (1950).
20. W. Imhof, R. Kalibjian, and V. Perez-Mendez, Rev. Sci. Instr. 29, 476 (1958).

21. M. Rich and R. Madey, Range-Energy Tables, UCRL-2301, March 1954.
22. D. Stork, Phys. Rev. 93, 868 (1954).
23. R. Martin, Phys. Rev. 87, 1052 (1952).
24. H. L. Anderson, W. C. Davidon, M. Glicksman, and U. E. Kruse, Phys. Rev. 100, 279 (1955).
25. D. B. Chelton and D. B. Mann, Cryogenic Data Book, UCRL-3421, May 1956.
26. M. Block, Phys. Rev. 101, 796 (1956).
27. L. S. Rodberg, (University of California) private communication.
28. W. R. Frazer and J. R. Fulco, Phys. Rev. Lett. 2, 365 (1959).
29. F. J. Dyson, Phys. Rev. 99, 1037 (1955).
30. G. Takeda, Phys. Rev. 100, 440 (1955).
31. R. Cool, O. Piccioni, and D. Clark, Phys. Rev. 103, 1082 (1956).
32. S. Barshay, Phys. Rev. 111, 1651 (1958).
33. L. S. Rodberg, Phys. Rev. Lett. (to be published)
34. E. A. Knapp, Angular Distribution of Photopions from Hydrogen, UCRL-8354 July 1958.
35. E. A. Knapp (Los Alamos) private communication.
36. R. M. Sternheimer, Rev. Sci. Instr. 25, 1070 (1954).
37. L. Eyges, Phys. Rev. 74, 1534 (1948).